DIGITAL INFRARED THERMOGRAPHY ANALYSIS FOR BREAST CANCER USING IMAGE TEXTURES FEATURES

NORLAILAH BINTI LANISA

FACULTY OF ENGINEERING
UNIVERSITY OF MALAYA
KUALA LUMPUR

2017

DIGITAL INFRARED THERMOGRAPHY ANALYSIS FOR BREAST CANCER USING IMAGE TEXTURES FEATURES

NORLAILAH BINTI LANISA

DISSERTATION SUBMITTED IN FULFILMENT OF THE REQUIREMENTS FOR THE DEGREE OF MASTER OF ENGINEERING SCIENCE

FACULTY OF ENGINEERING
UNIVERSITY OF MALAYA
KUALA LUMPUR

2017

UNIVERSITY OF MALAYA

ORIGINAL LITERARY WORK DECLARATION

Name of Candidate: Norlailah Binti Lanisa (I.C/Passport No:

Matric No: KGA14003

Name of Degree: MASTER OF ENGINEERING SCIENCE

Title of Project Paper/Research Report/Dissertation/Thesis ("this Work"):

DIGITAL INFRARED THERMOGRAPHY ANALYSIS FOR BREAST CANCER USING IMAGE TEXTURES FEATURES

Field of Study:BIOMEDICAL ENGINEERING

I do solemnly and sincerely declare that:

(1) I am the sole author/writer of this Work;
(2) This Work is original;
(3) Any use of any work in which copyright exists was done by way of fair dealing and for permitted purposes and any excerpt or extract from, or reference to or reproduction of any copyright work has been disclosed expressly and sufficiently and the title of the Work and its authorship have been acknowledged in this Work;
(4) I do not have any actual knowledge nor do I ought reasonably to know that the making of this work constitutes an infringement of any copyright work;
(5) I hereby assign all and every rights in the copyright to this Work to the University of Malaya ("UM"), who henceforth shall be owner of the copyright in this Work and that any reproduction or use in any form or by any means whatsoever is prohibited without the written consent of UM having been first had and obtained;
(6) I am fully aware that if in the course of making this Work I have infringed any copyright whether intentionally or otherwise, I may be subject to legal action or any other action as may be determined by UM.

Candidate's Signature Date:

Subscribed and solemnly declared before,

Witness's Signature Date:

Name:

Designation:

ABSTRACT

The number of breast cancer has been increasing over the decade. Multiple screening tools have been used to detect the cancer, such as mammogram, ultrasound, MRI, and thermography. Mammogram is the gold standard method for breast cancer screening. However, thermography screening method has caught the attention to be used as alternative screening tools due to its non-contact procedure as well as it is convenient for patients below 40 years old. In this study, thermography image will be used as the input image. The proposed method start by overlaying the binary ground truth (GT) mask with the greyscale thermography image to eliminate the background image. Then followed by manual extraction of the left and right breast into two similar size individual region of interest (ROI). Later, the ROI images contrast were improved by using histogram equalization (HE). From the equalized ROI images, three features were extracted namely Chi-squared distance, Earth Mover's Distance (EMD) and contrast measurement. Finally, the features will be tested using a paired t-test. This test was performed to analyse whether the features are statistically significant to classify the image into normal and abnormal classes. Based on the study done, Chi-squared distance and EMD features are statistical significance to be used in classification of normal and abnormal image. While, the contrast measurement is computed to be statistically insignificant for future classification work.

ABSTRAK

Bilangan kes penghidap kanser payudara telah meningkat sejak 10 tahun kebelakangan ini. Pelbagai jenis alat saringan telah digunakan untuk mengesan sel kanser, seperti mammogram, ultrasound, MRI, dan thermografi. Mammogram adalah kaedah standard untuk pemeriksaan kanser payudara. Walau bagaimanapun, kaedah saringan thermografi telah menarik perhatian para penyelidik yang mencadangkan kaedah ini digunakan sebagai teknik saringan alternatif berikutan prosedurnya yang tidak menyentuh pesakit serta sesuai untuk pesakit di bawah umur 40 tahun. Dalam kajian ini, imej thermografi akan digunakan sebagai input. Kaedah yang dicadangkan bermula dengan menindihkan imej thermografi berskala kelabu bersama imej rujukan binari untuk mengeluarkan bahagian latar imej. Selepas itu, bahagian kiri dan kanan payudara masing-masing akan diekstrak secara manual untuk mendapatkan kawasan berkepentingan (ROI) yang mempunyai saiz yang sama. Kemudian, kontras pada ROI diperbaiki dengan mengunakan kaedah penyamaan histogram. Lalu, ROI yang telah melalui proses penyamaan histogram akan digunakan untuk mengekstrak tiga maklumat iaitu 'Chi-squared distance', 'Earth Mover's Distance' (EMD) dan pengukuran kontras. Akhir sekali, maklumat-maklumat tersebut akan diuji dengan mengunakan 'paired t-test'. Ujian ini dijalankan untuk menganalisa samada maklumat-maklumat tersebut adalah nilai statistik yang signifikan untuk membezakan imej kepada dua kelas berbeza iaitu kelas normal dan sebaliknya. Berdasarkan kajian yang telah dijalankan, maklumat daripada 'Chi-squared distance" dan EMD didapati signifikan untuk digunakan dalam proses pengkelasan imej kepada imej normal dan imej tidak normal. Manakala, nilai pengukuran kontras pula tidak signifikan untuk digunakan dalam proses klasifikasi yang boleh dilakukan pada masa akan datang.

ACKNOWLEDGEMENTS

I would like to give my sincere gratitude to my advisors namely Dr Lai Khin Wee, Dr Ng Siew Cheok and Dr Hum Yan Chai for their continuous support and for their patience, motivation, enthusiasm and immense knowledge. I also deeply appreciate Dr Maheza and Dr Asnida from UTM for their valuable in my research. I would also like to thank all of my lab mates in Neuro Lab for all the motivation and fun we have had. I would like to thank my family for their unending support and encouragement throughout my study. Lastly, I would like to thank University of Malaya for the financial support offered.

TABLE OF CONTENTS

LIST OF FIGURES

LIST OF TABLES

LIST OF SYMBOLS AND ABBREVIATIONS

MRI	:	Magnetic Resonance Imaging
ROI	:	Region of interest
EMD	:	Earth Mover's Distance
HE	:	Histogram equalization
GT	:	Ground truth
CAD	:	Computer Aided Detection System

CHAPTER 1: INTRODUCTION

1.1 Introduction

Breast cancer is referred to the cells in the breast tissues that grow, change and multiply rapidly without control resulting to the formation of lump or mass. These masses are called tumour and can be either cancerous (malignant) or non-cancerous (benign). Malignant tumour is an invasive type of tumour which invade neighbouring tissues and spread to the other part of the body. Sometimes it also metastases, a condition where the tumour spread by move away from its original organ to another organ or bones. Benign cancer however didn't spread to other parts of the body and always in the condition where it is easy to be removed (Mookiah, Acharya, & Ng, 2012). Breast cancer usually start in the ducts, structures that carry milk from lobules toward the nipple or lobules, the milk glands.

Breast cancer is one of the most common cancers affecting woman. Based on the estimation in GLOBOCAN 2012 by the International Agency for Research on Cancer (Ferlay et al., 2015), 14.1 million new cancer cases and 8.2 million cancer deaths occurred worldwide. Lung cancer remains as the most common cancer with 1.8 million new cases (12.9% of total) follow by breast cancer with 1.7 million new cases (11.9%). The estimation for new cases in women population shows breast cancer is the most common cancer diagnosed, whether in more and less developed regions. More cases occurred in less developed countries with 883,000 cases compare to more developed regions with 794,000 cases (Ferlay et al., 2015). However, in mortality cases the rank of breast cancer different for developed and developing regions. In developed region, lung cancer is the leading cause of cancer death among women with 210,000 deaths followed by breast cancer (198,000 deaths). While for developing regions, breast cancer is the leading cause of cancer death (324,000 deaths) followed by lung cancer (281,000 deaths) and cervix cancer (230,000 deaths). The high number of new cases and death in developing regions

are believe due to multiple reasons. One of the reason is the non-availability of optimal breast cancer treatment in developing countries; small numbers of trained medical personnel, insufficient modern equipment, and high cost of cancer drugs. The other reasons are due to social barriers such as fatalistic beliefs, reluctance or refusal to be examined by a male doctor, fear of rejection by family and community, or affecting future marriage prospect (DeSantis et al., 2015).

In Malaysia, breast cancer is the leading cause of cancer-related deaths for females with 25% of all cancer-related deaths. The breast cancer mortality rates have been increasing 6% per year between 1997 and 2008 which is the largest recorded in Asia Pacific region (Youlden, Cramb, Yip, & Baade, 2014). Hence, to reduce the number of mortality due to breast cancer, early detection is crucial. Research has shown that 85% chance of cure if the tumour was detected earlier and only 10% chance if detected late (Qi & Diakides, 2009).

There are several imaging techniques use for detection and screening of breast cancer and the most commonly use are mammography, ultrasound and magnetic resonance imaging (MRI) (Onega et al., 2014). Among all, mammography is considered as the gold standard screening tool for breast cancer. This process uses system with low dose x-ray, high contrast and high-resolution film (Mookiah et al., 2012). Mammography detect any anatomical changes or structural distinction between tumour and breast tissue. However, mammography have several limitation. Firstly, the tumour must achieve certain size or thickness to be detected in mammogram. This cause the treatment to be delayed and reduce the chance of cure for the patient. Besides that, the density of the breast also affected the sensitivity of mammogram to differentiate between normal tissue and tumor. Mammogram also exposed patient with X-ray radiation which may destroyed the tissue or cause tissue mutation. Not to mention, mammogram procedure are time consuming,

cause physical discomfort and ineffective for surgically implanted breast or post-operative breast scar (Mookiah et al., 2012).

Due to the drawback of mammogram, a high interest have been given to thermography as breast cancer screening tool. Thermography did not use ionizing radiation, venous access or other invasive procedure (Moghbel & Mashohor, 2013). Besides that, it is a quick, painless, economic, risk free, and patient friendly imaging method. Therefore, it is suitable for all sizes and density of breast, pregnant or nursing women, implanted or non-implanted breast, and even post-operative patients. Thermography detected physiological changes by measuring the infrared radiation emitted by the body. Human body usually emitted narrow band wavelength of infrared radiation of 8 μm – 12 μm (Qi & Diakides, 2009). Breast normally produced symmetry temperature distribution. Cancer cells however cause asymmetry pattern in breast thermal image. The changes is because cancer cells released more heat by means of higher metabolic activity compare to surrounding tissue. Additionally, cancer cells increase local blood flow by producing chemicals to develop new blood vessels (angiogenesis) for food supply. This cause an increase of temperature to the area.

1.2 Objective

The main objective for this research is to extract features for normal and abnormal breast thermography images classification. Therefore, to achieve the main objective, two specific objectives are conducted namely:

i. To extract features that compare the left ROI and the right ROI.
ii. To analyse the significance of each features.

1.3 Dissertation Layout

This dissertation consists of five main chapters. The first chapter is the introduction, then followed by the second chapter. The second chapter consists of list of literature reviews discussing the previous work done on breast cancer as well as on computer aided design system for mammogram and thermogram image. The third chapter consists of the theory and procedures involved in the analysis of thermography images. Chapter four outlines the result as well as the discussion on the result obtained. Finally, the fifth chapter provides the conclusion and the suggestions for future works.

CHAPTER 2: LITERATURE REVIEW

2.1 Breast Cancer Anatomy

Breast organ overlaying the pectoral muscle of the chest. Women breast hold more adipose tissue (fatty tissue) than men and covers a large area starting from below the collarbone (clavicle) extended to the armpit (axilla) and across to the breastbone (sternum). Women breast are made up of lobules, ducts, areola, nipple, blood vessels, lymph nodes, lymph vessels and supported by muscle and ligament. Lobules are the glands that produce milks. A group of lobules will form lobes. Each women have around 15-20 section of lobes. Ducts are the tubes that carry milk to the nipple. Areola contains small sweat glands that secrete moisture during breast-feeding and nipple are the centre area for the milk comes out. There are four lymph nodes around breast area: superclavicular nodes, infraclavicular nodes, axillary nodes and internal mammary nodes (Johnson & Cutler, 2016). Figure 2.1 shows the female breast image.

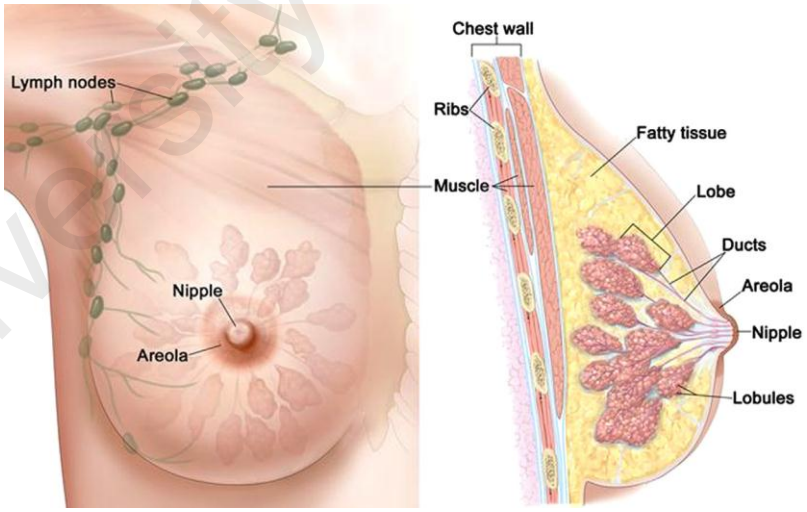

Figure 2.1: Female breast anatomy (Borchartt et al., 2013)

Understanding the anatomy of the breast is important to understand the growth of breast cancer. Breast cancer refers to the cells in the breast tissues that grow without control and proliferation rapidly, resulting in the formation of lumps or mass or also known as a tumour. There are two types of tumour. The first type is a malignant tumour.

An aggressive and cancerous type of tumour that invades its neighbouring tissue and spread to other parts of the body through blood vessels. Malignant types of cancer also metastasis by moving away from its original sites and growth in the new organ. The second type is a benign tumour. Benign tumour does not spread to other organs and in most of the cases, it can be easily removed through cancer treatment such as surgical. There are several types of breast cancer. Breast cancer that started in the duct known as ductal carcinomas. Lobular carcinomas are another type of carcinomas and this type started in lobules area. Around 10-15% of carcinoma cases are lobular carcinomas while nearly 80% are ductal carcinomas. Other types of breast cancer are colloid, medullary, micropapillary, papillary and tubular carcinomas as well as sarcomas; rare cancers developed from myofibroblasts and blood vessel cells. Different type of cancer will need different type of prognosis and treatment (Medicine, 2014).

There are several screening techniques for breast cancer screening such as clinical or self-examination, mammogram, ultrasound, magnetic resonance imaging (MRI), positron emission tomography (PET scan) and computed tomography (CT scan) (Rane, Joshi, & Chaudhari, 2014). Mammogram is the golden screening method for breast cancer.

2.2 Breast Mammography

As the most appropriate breast cancer screening tools nowadays, a large amounts of mammogram images are captured daily in hospitals and medical centres all over the world. Therefore, the radiologist is faced with difficulties to analyse and diagnose large numbers of image and are prone to perform errors due to fatigue. Therefore, a study by Shanthi and Murali Bhaskaran (2014) proposed a Computer Aided Diagnosis (CAD) systems to act as the second reader to detect abnormalities present in mammogram. A set of features based on Gabor filters, fractal analysis and multiscale surrounding region dependence method (MSRDM) are extracted to classify the mammogram into normal or benign or malignant. The classifier proposed is self-adaptive resource allocation network

(SRAN) classifier. The proposed method achieved 98.44% accuracy when trained and tested using 192 mammogram images.

Besides that, another group of researcher, Abdel-Nasser et al. (2015) also proposed a method to design a CAD system using mammogram image as an input. Figure 2.2 shows an example of the mammogram image used in their study. The CAD system design consists of three major steps, segmentation of ROI, features extraction and classification. The segmentation of ROI is done manually. The proposed features extracted is uniform local directional pattern (ULDP). The study shows the ULDP features able to characterize the breast tissue with 92.37% accuracy.

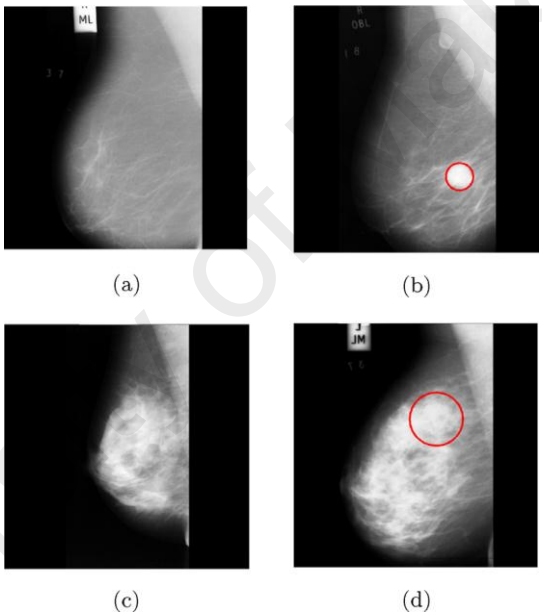

Figure 2.2: Examples of mammogram image fro mini-MIAS breast cancer database (Abdel-Nasser et al., 2015).

However, mammogram screening technique is less sensitive for below 40 years old women because of the breast tissue density (Moghbel & Mashohor, 2013). Besides that, the compression procedure in mammogram causes discomfort and painful experience to the patient. Therefore researcher try to come up with another alternative for breast cancer screening. One of the new modalities that attract quite high interest is thermography.

2.3 Breast Thermography

Thermography does not use ionizing radiation, venepuncture or other invasive procedures (Moghbel & Mashohor, 2013). Besides that, it is a quick, painless, economic, risk free, and patient friendly imaging method. Moreover, it is suitable for breasts of all sizes and density, of pregnant or nursing women, implanted breast, and even post-operative patients (Etehadtavakol, Ng, Chandran, & Rabbani, 2013). Besides that, thermography can detect smaller cancer cells around 12.8mm compare to mammogram around 16.6mm size (Ng, 2009). This will allow early detection of breast cancer all in all increase the chance of cure as stated by Qi and Diakides (2009) in their study that stated 85% chance of cure if the cancer detected earlier compare to 10% chance of cure if detected late.

Thermography detects physiological changes by measuring the infrared radiation emitted by the body. Human body usually emits narrow band infrared radiation of 8μm – 12μm wavelength (Qi & Diakides, 2009). Breast normally produces symmetrical temperature distribution. Cancer cells however cause asymmetrical patterns in breast thermal image. The changes are due to release of more heat by the cancer cells because of their higher metabolic activity compared to the surrounding tissue (Schaefer, 2014). In addition, cancer cells increase local blood flow by producing growth factors to develop new blood vessels (angiogenesis) for nutrition. This causes an increase in temperature of that area. Thermography instrument may produce a true colour image or a grayscale image. Figure 2.3 shown an example of thermography image.

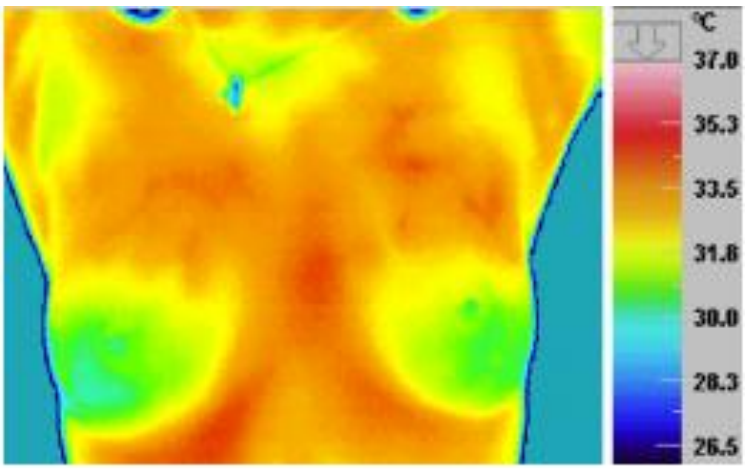

Figure 2.3: Thermography image (NG & KEE, 2007).

2.4 Image Acquisition

Araujo, Lima, and de Souza (2014) used camera FLIR S45 in their study. A data set of 50 patients from Federal University of Pernambuco Hospital, Brazil are obtained. Their patient were women aged 35 years and above with suspected masses with 14 patients have malignant masses, 19 patients have benign masses and 17 patients have cyst masses. The masses then confirmed by clinical examination followed by ultrasound, mammographic and biopsy exams. A written consent form signed by each patient. The protocol and apparatus suggested by Araujo et al. was registered at the Brazilian Ministry of Health and approved by the Ethics Committee of the Federal University of Pernambuco. The apparatus was designed and built to allow standard protocol to be conducted accurately and comfortably. The protocol that the patient will have to go through for image acquisition process were based on two categories of body heat transfer behavior; static and dynamic. Two hours before image capturing, patients were advised not to smoke, consume caffeine or alcohol, do any physical activities, and apply cream or ointment on breast area. At the time of capturing the image, patient body temperature was recorded and any accessories present, were taken off. For static acquisition, the first step was to make the patient seated on the bench for 10 minutes with her arms on the armrest to stabilize body temperature with the surrounding temperature. During these 10 minutes, atmospheric temperature and relative humidity were observed. The image was then

captured with patient standing 1.0 meter from the infrared camera and hands over her head. For dynamic acquisition, a cooling fan was directed to the breasts with arms above her head. The fan was then turned off when the temperature around the chest central region dropped to less than 30.5ºC and finally the image of the breasts was captured.

Study done by Wishart et al. (2010a) however is different from the previous researcher. In this study, 100 patients and 106 biopsies were obtained when thermography conducted in the Cambridge Breast Unit, Addenbrooke's Hospital. The patient were age between 33 until 87. 65 patient were diagnose with malignant cases and 41 patient under benign cases were confirmed by mammography, ultrasound and MRI. All the patient sign consent form. For their protocol, local Research Ethics Committee were the committee responsible for giving the approval. However, not all patient are involve in the research. The researcher excluded some patient that have breast cancer surgery or treatment before, loss one or both nipples, over 113kg weight and acute breast inflammation. Before capturing patient thermal image, patient need to disrobe to the waist and seat with arm supported at eye level. For 5 minutes, air flow were directed to the breast to allow the body surface temperature to drop until it achieve equilibrium with the surrounding temperature. At the same time, thermal camera recorded the changes of skin surface temperatures for a total of 250 individual frames. Thermal image were capture using Sentinel BreastScan by Infrared Sciences Corp.

Krawczyk and Schaefer (2014) and Schaefer, Závišek, and Nakashima (2009) used 146 thermograms data set in their study with 29 shown malignant cases and 117 shown benign cases. However, the protocol and the camera used in this study were not stated in any part of the paper. In EtehadTavakol, Chandran, Ng, and Kafieh (2013) study, 32 images of 9 malignant, 12 benign and 11 normal cases compiled from multiple places named Ann Arbor Thermography Center, Thermal Imaging Lab in San Francisco Bay Area, American College of Clinical Thermology, Thermography of Iowa, Sun State

Thermal Imaging Center in Australia and Department of Diagnostic Radiology, Singapore Genera Hospital. They however suggested several rules for image acquisition. The patient must stand 1m from the thermal camera. Room temperature must be around range 20-22ºC with humidity at 60 ± 5%. The patient must stay in the room and stay seated for 15 minutes to stabilize and reduce the basal metabolic rate achieve minimum surface temperature changes. The patient must wear loose gown and within the period of the 5^{th} to 12^{th} and 21^{st} day after her menstrual cycle onset.

Acharya, Ng, Tan, and Sree (2012) obtained their thermography image from Singapore General Hospital. NEC-Avio Thermo TVS2000 MkIIST System was the instrument use to capture the patient thermography image. The instrument was placed 1m from the patient. Patients were required to stay in a temperature controlled room (20-22ºC) with humidity of 60 ±5% wearing loose gown. Patients stayed for 15 minutes in the room to stabilize their body temperature with the surrounding temperature hence minimal surface temperature changes on breast surface temperature during the experiment. Another condition was the patient was on period of the 5^{th} to 12^{th} and 21^{st} day after her menstrual cycle onset. 50 patient thermography images use in this study with 25 thermograms from cancer patients and 25 images of normal patients. For the cancer patients, 15 images shown the heat surface pattern of patient that had stage 3 cancers and 10 images of patient with stage 2 cancers.

Suganthi and Ramakrishnan (2014) used online database developed by team Araujo et al. (2014) for their study. Besides the original thermography, its corresponding ground truth images were also collected from the online database. These images were the result of manually cropping the region of interest (ROI) by radiologist and specially trained personnel. 35 images were tested for this work.

A review by Borchartt et al. (2013) listed several types of acquisition protocols and number of acquisition and database use. For static acquisition, some researches requires

their patient to stabilize their body temperature by staying in a controlled room for around 10 to 20 minutes. For dynamic acquisition, most researchers used fan to cool the breast area while capturing the breast images in between 4 to 20 minutes. The controlled room temperature and humidity were varied due to the location where the image were captured. Some researcher even include special recommendation to increase the reliability of the images captured in their study. The protocols they set required the patient to avoid alcohol, caffeine, skin products, smoking and doing any physical activities 2 hours before the test.

The review also shown the number of patients involve in thermography test. The highest number of patient was 220 patients. Some work involved the designing of equipment for patient positioning. Number of images captured for each person also varies. Even though, the lateral images were also captured, all testing usually involve the frontal images only.

Based on all the image acquisition stated above, a lot of acquisition protocols were introduced. However, there were several similarities among all the protocols such as the distance between infrared camera and patient as well as the restrictions that must be followed by patient two hours before the test. These similarities might bring to the making of standard protocols for thermography in the future.

2.5 Image Processing

Araujo et al. (2014) used manual segmentation in their study to avoid errors due to the natural asymmetry of human body heat pattern. In their study, they used FLIR ThermaCAM Quick Report software (propriety software by FLI Infrared System Manufacturer) to produce a digital thermal image with two different component. The first one was temperature matrix and the other was color map pattern. The temperature matrix registered the temperature value of pixel of the image. This allow them to have the temperature information instead of the intensity of the pixel. By using Matlab software,

ellipsoidal elements used to select area of interest for each breast. Manual adjustment was done to obtain the optimum breast area. Temperatures matrices obtained for each breast respectively then processed using morphological processing to obtain localized temperature increase (LTI). The morphological processes that involve were erosion, top hat transformation, dilation. Two matrices containing morphological information for each breast were obtained for feature extraction.

Krawczyk and Schaefer (2014) and Schaefer et al. (2009) also used manually segmented image by medical expert for their study. EtehadTavakol, Chandran, et al. (2013) studied different image processing step to separate both breast areas from the background. The first step was using Canny edge detector to detect the edge of the lower boundaries of breasts and the edge of torso. Only the outermost boundaries will be kept for the next process. The intersection between both breast lower boundaries mark as the high curvature point. Another end of the each breast lower boundaries mark as another high curvature points. All the high curvature point plus another 6 landmark points connected to form the exact lower breast boundaries to extract the breast area from its background. The location of this points were learned using training algorithm and 20 breast images. The image segmentation method used acquire 90% precision when tested with the available images.

Krawczyk and Schaefer (2014) work involved 3 major image segmentation steps for its automatic segmentation process. The initial step was non-linear isotropic diffusion filter. The algorithm developed for this step used to preserve, brighten and sharpen the edges in the image. Next step was level set method without re-initialization. External energy term was used to detect the desired object boundaries. By using the level set function, edge function, univariate Dirac function, Heaviside function and image data as the input, the curve of the object boundaries was detected via several development. ROI obtained according to the boundaries. Lastly, the ROI verified and validated using the

comparison result between the ROI obtained through all the process and the ground truth area image. The values of accuracy, sensitivity, specificity, true positive and true negative use to analyze the correlation between both images. The author managed to get 98% correlated images.

Borchartt et al. (2013) in their work summarize the degree of segmentation by previous researches in their review. Looking into the level of automation, out of 13 works reviewed by the author, 8 team designed fully automatic system for the detection of breast cancer. This were due to the lack of expertise in this field and also to reduce any human error during the classification of the images.

2.6 Feature Extraction

Araujo et al. (2014) in their study, extracting thermal interval features. By extracting the interval feature extraction, four dimensional interval feature vector is obtained. This features then used to extract four continuous features. By using the span and content components of the Gowda-Diday dissimilarity measure between two intervals, they manage to obtain a continuous feature vector. Next, they extracted the feature of space transformation based on the Fisher's criterion. The transformation matrix based on the Fisher's criterion constructed after several training. Then the transformation matrix will transform continuous feature vector into bi- dimensional feature vector.

Krawczyk and Schaefer (2014) used different method for their feature extraction. First, the breast areas segmented convert to polar coordinate. Then, statistical features calculated to indicate symmetry properties of both breast area. Mean, standard temperature deviation, median, the 90 percentile, the absolute difference between both breast are the features obtain in this step. Then, four elements in image moments, the absolute difference between both breasts calculated to be used as feature. Histograms that show the frequency of certain temperature allowed the cross-correlation, absolute value of its maximum, the numbers of bins exceeding a certain threshold, the number of zero

crossing, energy and the difference between the positive and negative part of the histogram to be obtained. Next is the co-occurrence matrix. Homogeneity, energy, contrast, symmetry, first four moments of the matrix were the features extracted. Mutual information calculated from joint entropy and the Fourier transform to get the difference maximum value for both breast area, the distance of this maximum from the center were the features to be extracted. By filtering the image using Laplacian filter to enhance the thermography image allow researcher to obtain another set of features from the resulting images. Overall there were 38 features extracted in this study.

Acharya et al. (2012) used texture analysis to obtain their features. This analysis measures the smoothness and regularity of pixels in images. It will show the relationship between intensity values of pixels. The first group of features were calculated from the co-occurrence matrix for example entropy, contrast and correlation. The second group was run length matrix. Gray level non-uniformity and run percentage were some of the features extracted under this group. Overall, 16 texture features were extracted.

Besides of all the features extraction methods listed above, review by Borchartt et al. (2013), mostly stated the used of statistical features as their main information in classifying the cancer stages shown in thermography.

2.7 Image Classification

Araujo et al. (2014) considered linear discriminant classifier, minimum distance classifier based on Mahalanobis distance, minimum distance classifier based on Euclidean distance, minimum distance classifier based on City-block distance, Parzen window. The result then compared with statistical asymmetry feature extraction and texture feature extraction. The statistical feature were the mean, variance, skewness, kurtosis, entropy, and histogram. The texture features were run percentage, contrast, correlation, energy and homogeneity. The error rate were 32%, 30%, 38%, 84% and 36%

respectively to the classifier listed above. The choice of classifier was not discuss in the paper.

Wishart et al. (2010b) analyzed the infrared scans in four ways; Sentinel screening, sentinel neural network, NoTouch software and expert manual review. Expert manual review have sensitivity 78% and specificity 48%. Sentinel screening have sensitivity 53% and specificity 41%. For Sentinel Neural network the sensitivity was 48% and specificity was 74%. NoTouch BreastScan get sensitivity 70% and specificity 48%. Compare to other modalities, mammography sensitivity was 89% and ultrasound sensitivity and specificity were 90% and 95% respectively. The combination of mammography and NoTouch BreastScan increased the sensitivity to more than 89%. Therefore, it is proven that DIB was useful when use together with mammography.

Krawczyk and Schaefer (2014) classification was based on the classification of features obtained. They used multiple classifier system (MCS) which train base classifier such as standard single support vector machine (SVM), bagged SVM, boosted SVM, a random forest classifier, SMOTEBagging and SMOTEBoost. All possible and sensible combination is considered. The best performance correctly identified malignant cases three times more with 80.35% sensitivity, 90.15% specificity and 90.03% accuracy compare to fuzzy classifier optimized by genetic algorithm, 79.86% sensitivity and 79.49% specificity and ant colony optimization classifier accuracy 79.52%. It is proven neural network fusion gives better result compare to classifier based on evolutionary computing

Schaefer et al. (2009) in their study used fuzzy rule-based classification for pattern classification. It was a supervised process that involved two steps. The first step is to get the antecedent part. The author derived their classifier by training a set of data to categorize the data manually. The second step was to acquire the consequent part which was the information obtained by analyzing the training pattern. Then, the classifier tested

with the training set again and the sensitivity and specificity for 10 – 15 fuzzy partitions were recorded. Even though the classifier tested using the same data as the training data, the highest number of sensitivity and specificity were only 93% and 98% respectively at 15 fuzzy partition. The classifier then tested again using their test data with the same number of partitions. The highest was at 14 partitions where the sensitivity and specificity got almost 80%. They concluded thermography as a useful aid for diagnose and will be more powerful when use together with mammogram.

Acharya et al. (2012) used another type of classifier which was Support Vector Machine (SVM) for pattern recognition. They used three fold stratified validation method. Firstly they split their dataset into 3 group. 2 group was used as the training set to develop the classifier algorithm and the other group was used as the testing set. The whole procedures were repeated three times using different testing set for each time. The result of their testing were 88.10% accuracy, 85.71% and 90.48% sensitivity and specificity respectively. The author suggested that improvement can be settled by extracting better features and use larger number of data sets.

2.8 Summary

As a conclusion, lots of studies have been done to bring forward thermography as clinical screening method. However, to the best of my knowledge, the complex intensity of thermography causing the difficulty for researcher to segment out the area with the highest temperature and the region of interest which in this case are the right and left breast. Therefore, manual segmentation is considered as the best choice for segmenting right breast and left breast. This segmentation will then followed by analysing each breast image to extract possible features for classification process.

For feature extraction, previous study use statistical features, texture features and pattern recognition features to calculate the asymmetry properties between left and right thermography breast image. In this study, the comparison features between both sides of

breast image were computed using distance measurement and contrast measurement. The significance of this features were then calculated using paired t-test. The significance value are important to analyse the suitability of each features for future classification work.

CHAPTER 3: METHODOLOGY

3.1 Image Acquisition

140 grayscale thermography images were used as the data sets comprising of 90 images for healthy patients and 50 images for sick patients with possibility of benign or malignant cancer on one breast. The images and its corresponding ground truth (GT) mask were obtained from an online database by Visual Lab (Marques, Resmini, Conci, Fontes, & Lima, 2012). The GT masks were binary images with pixel value of 0 and 1. The resolution for both image group was 320 x 240 pixels with its format set as Portable Network Graphics (.png) image.

The thermography images were captured in University Hospital of UFPE (Brazil). The images then stored in an online database. The acquisition procedure has been approved by Ethical Committee of UFPE and the storage of images registered at Brazilian Ministry of Health. The patients were instructed to follow several procedure before the image acquisition. Patients were refrained from smoking, consuming caffeine and alcohol, conducting any physical activities and applying ointment on breast area two hours before image acquisition. There were two procedures for image acquisition: dynamic and static. The images were also captured from different position; frontal, 45º of the right side, 45º of the left side, 90º of the right side and 90º of the left side. Infrared camera were placed 1.0 meter from where the patients seated to attain clear image (Lanisa, Cheok, & Wee, 2014). For this study however, only frontal view images captured via static procedure were used. Frontal view images captured by directing the infrared camera to the chest area to obtain an image comprising both breast. Thus, left breast and right breast region of interest are extracted from the same image. For static procedure, patient were seated for 10 minutes with both arms resting on the supports designed by the researchers. This procedure was performed to stabilise the skin surface temperature. Unlike normal tissues, the surface temperature for possible cancer region were persistent to balance with

surrounding temperature. Hence, the infrared emission from this region will show abnormal pattern on thermal image (Francis, Sasikala, Bharathi, & Jaipurkar, 2014).

3.2 Image Segmentation

Segmentation of breast region was performed manually by overlaying raw grayscale image with its respective GT mask. The GT mask accentuated the region of interest (ROI) by retaining the pixel value inside the ROI and lessen the value outside the ROI into 0. The ROI referred to the breast area and the region above the breast. Then, using two identical square cropped box with the size of 110 x 110 pixels, equal size of left breast ROI (ROIL) and right breast ROI (ROIR) were extracted as shown in Figure 3.2 and Figure 3.3. Figure 3.1 shows the flow chart for image segmentation process. Figure 3.2 shows an example of manual cropping process for healthy patient normal image while Figure 3.3 show an example to extract ROI in abnormal images.

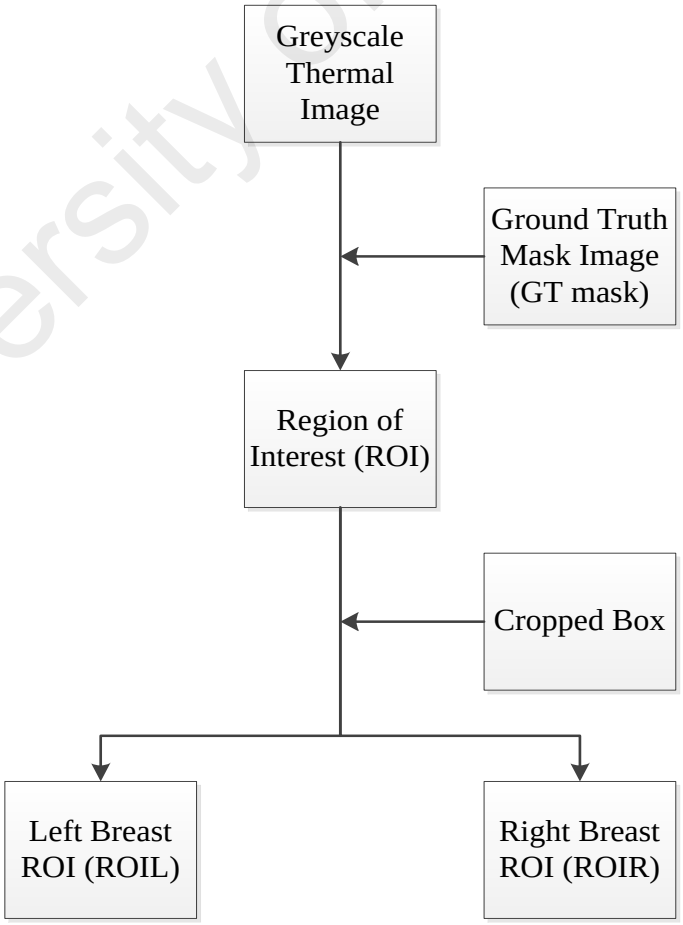

Figure 3.1: Image segmentation flowchart.

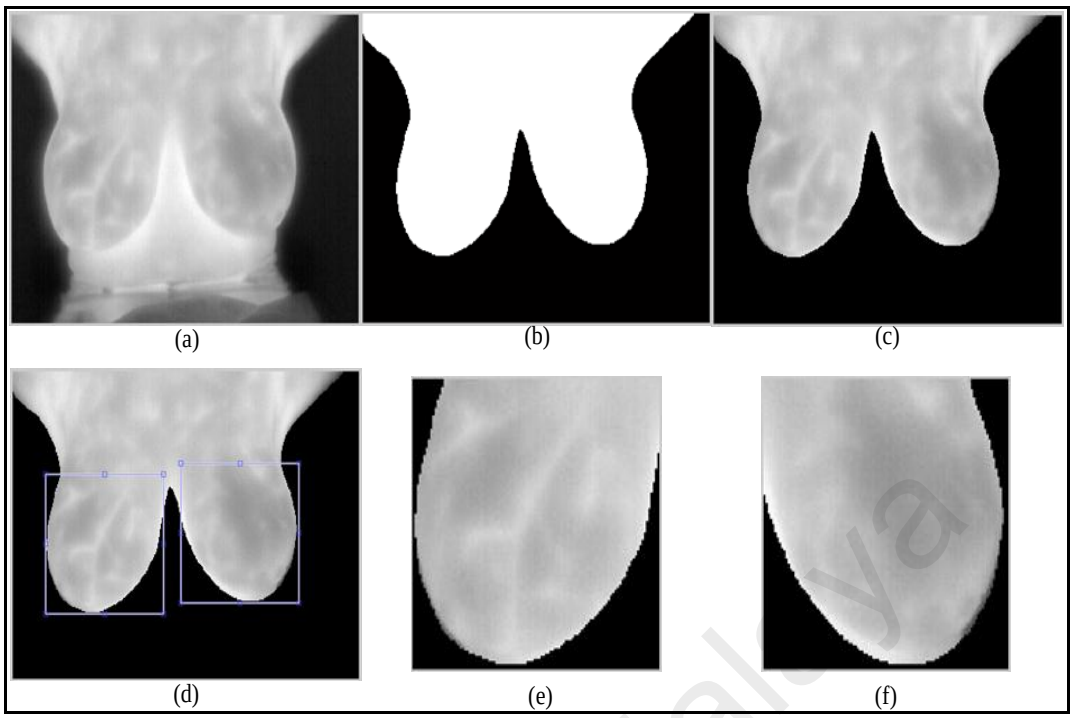

Figure 3.2: Normal image. (a) Original image, (b) ground truth image, (c) ROI image, (d) cropped box on both side, (e) right breast ROI and (f) left breast ROI.

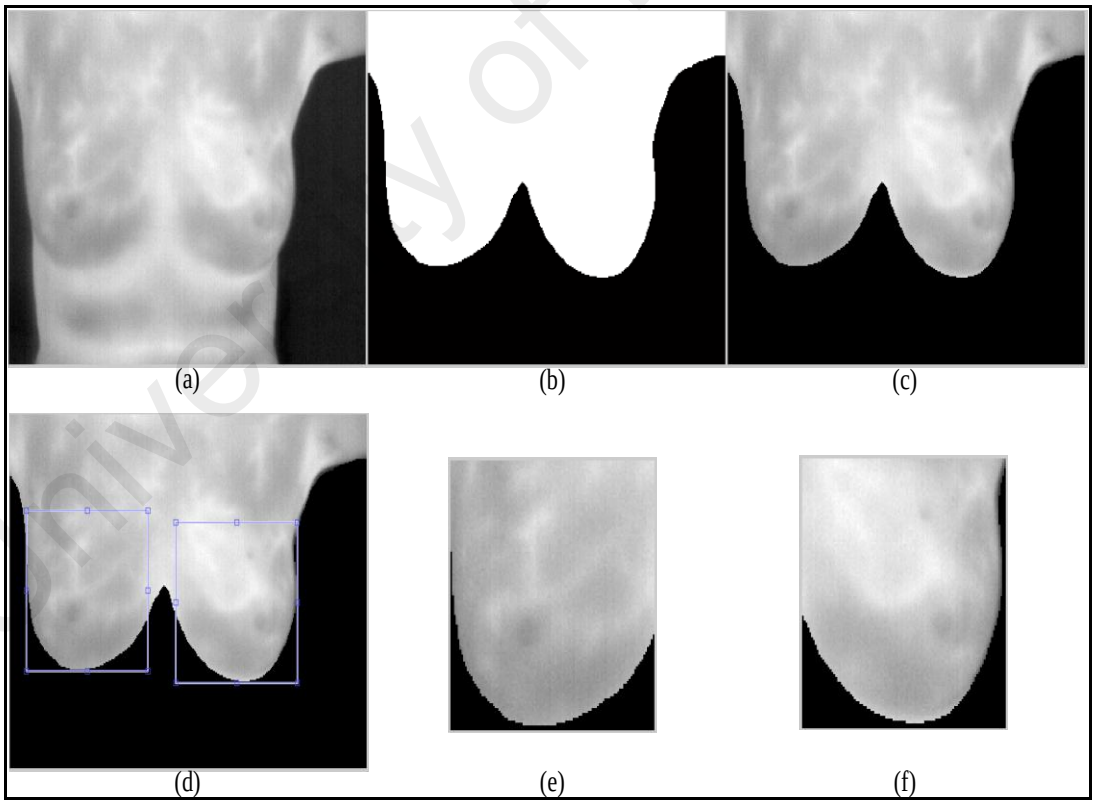

Figure 3.3: Abnormal image. (a) Original image, (b) ground truth image, (c) ROI image, (d) cropped box on both side, (e) right breast ROI and (f) left breast ROI.

3.3 Histogram Equalization

Prior to the features extraction of histogram distance and contrast measurements, both $I_L(x,y)$ and $I_R(x,y)$ undergoes a pre-processing process of histogram equalization (HE) to enhance the contrast and to standardize the grayscale distribution of both ROIs. The $I_L(x,y)$ represented the pixel intensity on coordinate (x,y) of segmented ROIL and $I_R(x,y)$ represented the pixel intensity on coordinate (x,y) of segmented ROIR. Firstly, the probability density function (PDF) of each discrete pixel intensity bin computed using equation 3.1 for ROIL and equation 3.2 for ROIR.

$$P_L(k) = \frac{n_k^L}{T^L} \qquad 0 \le k \le G-1 \tag{3.1}$$

$$P_R(k) = \frac{n_k^R}{T^R} \qquad 0 \le k \le G-1 \tag{3.2}$$

G denoted the total number of discrete bins, T^L and T^R denoted the total number of pixels in I_L and I_R respectively, n_k^L and n_k^R denoted the total number of pixels with gray intensity k in I_L and I_R respectively. Next, the cumulative distribution function (CDF) of P_L and P_R denoted as C_L and C_R computed respectively.

$$C_L(k) = \sum_{k=0}^{k=G-1} P_L(k) \tag{3.3}$$

$$C_R(k) = \sum_{k=0}^{k=G-1} P_R(k) \tag{3.4}$$

Then, the histogram equalized output for both images, denoted as I_{EL} and I_{ER}, computed by transforming each discrete grey pixel intensity in original ROIs to a new discrete grey pixel intensity according to the CDF defined in equation 3.3 and equation 3.4 as follows:

$$I_{EL}(x,y) = \lfloor (G-1) C_L(I_L(x,y)) \rfloor \tag{3.5}$$

$$I_{ER}(x,y) = \lfloor (G-1) C_R(I_R(x,y)) \rfloor \tag{3.6}$$

3.4 Image Analysis

Three features extracted in this study namely Chi-squared distance, Earth Mover distance and contrast measurements.

3.4.1 Chi-Squared Distance

The first features extracted in this study was Chi-squared distance. The Chi-squared histogram distance was a bin-to-bin distance measurement that used to compare the level of discrepancy between the grey level pixel intensity distribution value of both ROIR and ROIL. The Chi-squared histogram distance between I_{EL} and I_{ER}, denoted as $D(I_{EL}, I_{ER})$, was defined as follows:

$$D(I_{EL}, I_{ER}) = \sum_{k=1}^{k=L-1} \frac{[P_{EL}(k) - P_{ER}(k)]^2}{P_{EL}(k) + P_{ER}(k)} \quad (3.7)$$

Equation 3.7 results in an unbounded metrics of histogram distance measurement. Therefore, to bind the metric, the Chi-squared histogram distance was modified to form equation 3.8.

$$D(I_{EL}, I_{ER}) = \sum_{k=1}^{k=L-1} \frac{[|P_{EL}(k) - P_{ER}(k)| + C]^2}{P_{EL}(k) + P_{ER}(k) + (1+C)^2 - 1} \quad (3.8)$$

In equation (8), P_{EL} and P_{ER} denoted the PDF of I_{EL} and I_{ER} respectively and *C* denoted any constant larger than unity resulting in a bounded range: $(1 + C)^2 < D(I_{EL}, I_{ER}) < 0$. Chi-squared histogram distance quantifies the discrepancy between two images according to their discrete gray intensity. As compared to Euclidean distance, Chi-squared distance emphasizes that difference in high value bin is less important than difference found in small value bin. The higher the distance value, the larger the difference between two images. For example, in this study, for normal cases, the D value should be smaller and vice versa for abnormal cases. Later, to reduce the sensitivity to bin location, a cross-bin distance measure was adopted to measure the level of similarity between two histograms.

3.4.2 Earth Mover's Distance (EMD)

Second feature was Earth Mover's Distance or simply EMD. EMD was a histogram distance metric based on the solution of transportation problem (Monge-Kantorovich problem) (Rachev, 1985), in which quantifies the dissimilarity between two distributions in multi-dimensional feature space. It was named as Earth Mover's distance because the problem can be imagined as filling holes with piles of earth mass by a transport in which the histograms to be compared can be viewed as hole or earth mass. Mass was often used to represent the histogram weight because the EMD solution was related to an optimization problem known as mass transfer problem. The size of the holes or the amount of the earth mass was represented by the value of corresponding histogram bin. The distance between each hole and pile of earth mass (represented as $\mathbf{D} = [d_{i,j}]$) travelled by the transport multiplies with the load carried by the transport equals to the work done for that particular move in which one unit of work equals to one unit of distance of travelling with one unit of load. The EMD can then measures the least total work to be done in order to fill the holes with the mass of earth. The higher the value of EMD, the higher the value of minimum work must be done to complete to change one distribution of histogram to the other histogram. In cases where both histograms containing identical total weights, either of the histogram can be viewed as hole or pile and this optimization process can be viewed as weights flowing between both histograms until both distributions becomes the same.

The value of EMD between I_{EL} and I_{ER} can be viewed as a cross-bin similarity measurement between two pixel intensity distribution; if the distance is large, it indicates some degree of abnormalities exist. The histogram that contains higher brightness mean and contrast then would identifies as the side of breast that might be suspicious. The normalized histogram of ROIL with discrete gray scale intensity value *i* represented by $P_{EL}(i)$ and $P_{ER}(j)$ represented the normalized histogram of ROIR with discrete gray scale

intensity value j. Firstly, to compute the value of EMD between two distributions, I_{EL} and I_{ER} were formalized into a linear programming problem in which the purpose was to find mass (represented as $\mathbf{F} = [M_{i,j}]$) in each move carried by the transport between each pair of bin in $P_{EL}(i)$ and $P_{ER}(j)$ such that it minimizes the following cost function:

$$WORK(I_{EL}, I_{ER}, \mathbf{F}) = \sum_{i=1}^{i=L-1} \sum_{j=1}^{j=L-1} d_{ij} M_{i,j} \qquad (3.9)$$

Subject to the following constraints:

(i) The mass carried in each move must at least equals to nothing but not negative.

$$M_{i,j} \geq 0 \qquad 0 \leq i \leq L-1, 0 \leq j \leq L-1$$

(ii) The total mass carried from each particular bin in $P_{EL}(i)$ to all the bins (or holes) of $P_{ER}(j)$ (where *j* ranges from 0 to L-1) must less than the maximum value in that particular bin in $P_{EL}(i)$:

$$\sum_{j=0}^{L-1} M_{i,j} \leq P_{EL}(i) \qquad 0 \leq i \leq L-1$$

(iii) The total volume of each hole in each particular bin in $P_{ER}(j)$ that can be filled from all the bins from $P_{EL}(i)$ (where *i* ranges from 0 to L-1) must less than the maximum value in particular bin in $P_{ER}(j)$:

$$\sum_{i=0}^{L-1} M_{i,j} \leq P_{ER}(j) \qquad 0 \leq i \leq L-1$$

(iv) The total flows of each possible pair must be equal to the minimum of either histogram distribution:

$$\sum_{i=0}^{L-1} M_{i,j} \leq min(\sum_{i=0}^{L-1} P_{EL}(i), \sum_{j=0}^{L-1} P_{ER}(j)) \qquad 0 \leq i \leq L-1$$

The optimal $\mathbf{F} = [M_{i,j}]$ attained by solving the transportation problem of equation 3.9 enable the work to be done minimally. The Earth Mover's Distance (EMD) then computed by normalizing the minimum work calculated using equation 3.9 by the weight of the distribution with lesser total weights of histograms which in this study, both histograms contain same amount of weights ::

$$EMD(P_{EL}, P_{ER}) = \frac{\sum_{i=1}^{i=L-1}\sum_{j=1}^{j=L-1} d_{ij}M_{i,j}}{\sum_{i=1}^{i=L-1}\sum_{j=1}^{j=L-1} M_{i,j}} \quad (3.10)$$

The problem in this study was considered as EMD in one-dimensional of equal weights since only pixel intensity was considered and the size of both the ROIs was identical. Thus, the value of EMD was able to be computed efficiently based on the fact that the minimum work to be performed in order to transform one distribution into the other distribution can be computed as the area difference between the CDFs of both distributions.

3.4.3 Contrast Measurement

The final features extracted was contrast measurement. The contrast measurement used to calculate the amount of randomness in each of the ROIs. The measurement of contrast was approximated using the standard deviation of each of the discrete grey intensity in ROI as compared to the average grey intensity value computed for the entire image excluding the background.

Segmented image denoted as $I_{masked}(x, y)$ with size M x N with M denotes the number of column and N denotes the number of row. The mean of I_{masked} represented by μ(I_{masked}) defined as following:

$$\mu = \frac{1}{\mathbf{T}_\mu}\sum_{x=1}^{x=M}\sum_{y=1}^{y=N} I_{masked}(x, y) \quad (3.11)$$

$$\text{where } \mathbf{T}_\mu = \sum_{\boldsymbol{i=1}}^{\boldsymbol{i=}} [\![I_{masked}(x, y) > 0]\!] \text{ and } \mathbf{T}_\mu \neq 0$$

The μ(I_{masked}) computed the average value of I_{masked} by considering only on the pixel values which are not zero as $\mathbf{T}_\mu$ represented the total number of pixels which are larger than zero. The $I_{EL}(x, y)$ and $I_{ER}(x, y)$ denoted the ROIR and ROIL with size of $S_1 \times S_2$ where S_1 denoted the number of column and S_2 denoted the number of rows. This

mean then used to construct the contrast of $I_{EL}(x,y)$ and $I_{ER}(x,y)$ represented as C_{EL} and C_{ER} as shown in equation 3.12 and 3.13.

$$C_{EL} = \frac{1}{\mathbf{T}_C}\sqrt{\sum_{x=1}^{x=S_1}\sum_{y=1}^{S_2}[I_{EL}(x,y) - \mu]^2} \tag{3.12}$$

$$C_{ER} = \frac{1}{\mathbf{T}_C}\sqrt{\sum_{x=1}^{x=S_1}\sum_{y=1}^{S_2}[I_{ER}(x,y) - \mu]^2} \tag{3.13}$$

$$where\ \mathbf{T}_C = (S_1)(S_2)$$

The contrast value quantified the approximated randomness in the ROI taking the overall gray-scale average value as reference. The dependency of C_{EL} and C_{ER} norm values on the background gray-scale contrast, C_{Base}, of the image, can be defined as followed:

$$C_{Base} = \frac{1}{\mathbf{T}_\mu}\sqrt{\sum_{x=1}^{x=S_1}\sum_{y=1}^{S_2}[I_{masked}(x,y) - \mu]^2} \tag{3.14}$$

Next, within the reasonable range of discrepancy, the comparison between C_{Base} and contrast in ROIs computed as followed.

$$R_{B/L} = \frac{|C_{Base} - C_{EL}|}{C_{Base} + C_{EL} + e} \tag{3.15}$$

$$R_{B/R} = \frac{|C_{Base} - C_{ER}|}{C_{Base} + C_{ER} + e} \tag{3.16}$$

$$\text{Contrast} = \frac{|R_{B/L} - R_{B/R}|}{R_{B/R} + R_{B/L} + e} \tag{3.17}$$

The comparison between C_{Base} and C_{EL} was represented as a ratio denoted as $R_{B/L}$ and comparison between C_{Base} and C_{ER} was denoted as $R_{B/R}$.The real value e represents arbitrarily small value of constant to assure computational stability. Both $R_{B/L}$ and $R_{B/R}$ ranges from 0 to 1. The ratio gets larger if the contrast of the particular ROI was very different from the base contrast. The process of contrast analysis then computed further to obtain the contrast value. The contrast value extracted from abnormal images would have higher value compared to features extracted from normal images.

3.5 Features Analysis

The next process were to analyse the features extracted significance in differencing between normal and abnormal cases. The extracted features were subjected to the dependent samples t-test or also called paired t-test. The paired t-test were used to compare the means between two groups of data which can be paired with one another.

For every patient, three features values (Chi-squared Distance, EMD, and contrast measurement) were evaluated in pair. Prior computing the paired t-test, the results of each feature were rearranged into two groups. The grouping of data were based on its contrast value where the first group have the lower value of contrast of ROI (Group 1) and the second group have the higher value of contrast of ROI (Group 2). In order to validate the paired t-test, the feature values for each group were distributed normally. The normality test using D'Agostino test performed to gauge the discrepancy from normality using D statistic:

$$D = \frac{\sum(i-\frac{n+1}{2})X_i}{\sqrt{n^3 SS}} \tag{3.18}$$

Symbol *D* in equation 3.18 represented the test statistics, the n denoted the sample size, *i* denoted the observation rank of *X*, and *SS* denoted the sum of squares of the data.

CHAPTER 4: RESULT AND DISCUSSION

This chapter focuses on the results that were obtained based on the methodology described in Chapter 3. Also, this chapter discusses the results presented in Table 4.1 and Table 4.2 on the significance of each feature extracted. This chapter is divided into two sections and several subsections.

4.1 Histogram Equalization

The result of HE is shown in Figure 4.1 until Figure 4.20. ROIR shows the extracted image for right breast ROI and ROIL shows the extracted images for left breast ROI. IEL and IER shows equalized images of ROIR and ROIL respectively. Figure 4.1 until Figure 4.10 shows the HE result for images from normal case and Figure 4.11 to Figure 4.20 shows the HE result for images from abnormal case.

4.1.1 Result From Normal Cases

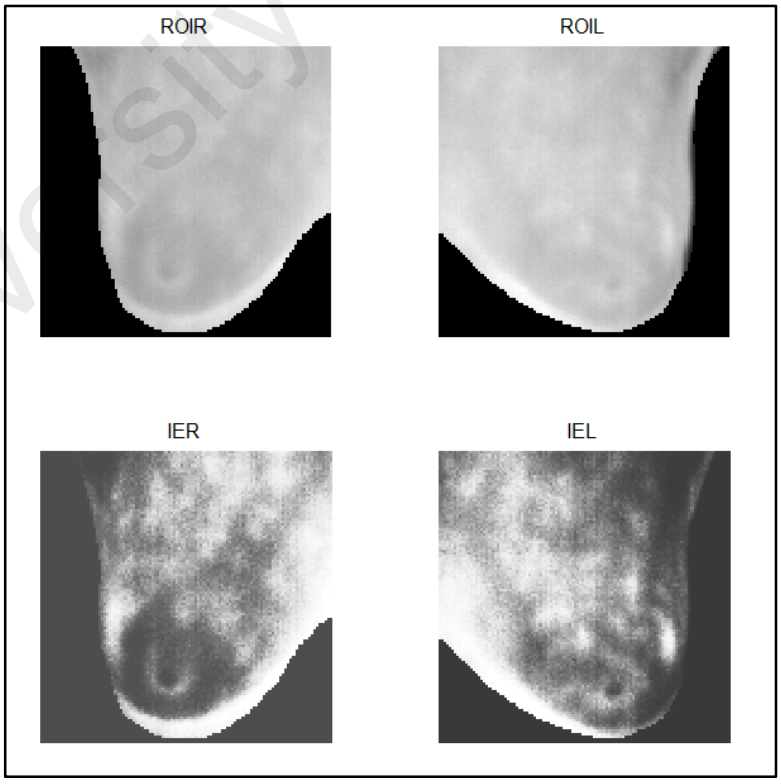

Figure 4.1: Original images and equalized images for Patient N08.

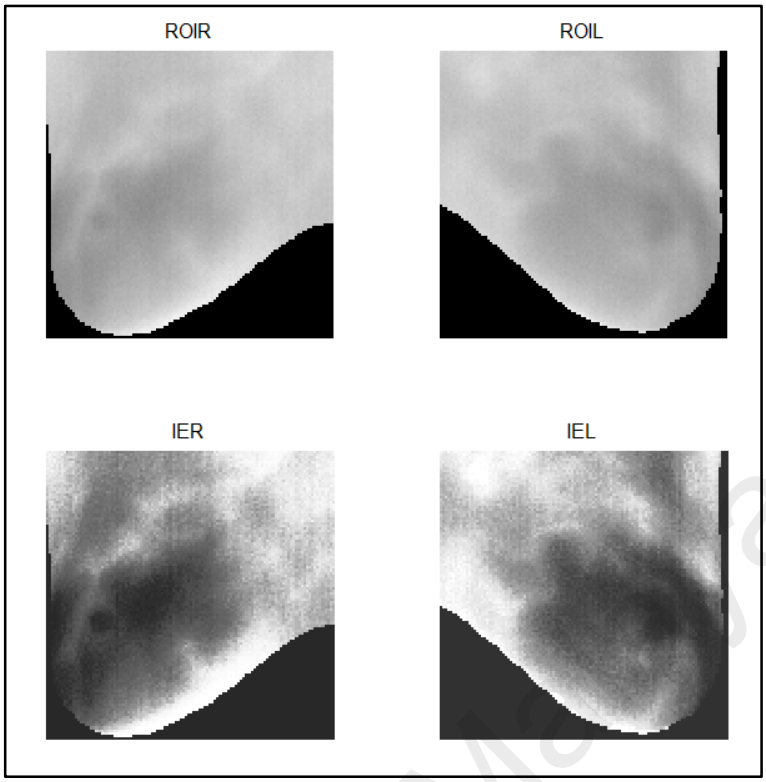

Figure 4.2: Original images and equalized images for Patient N15.

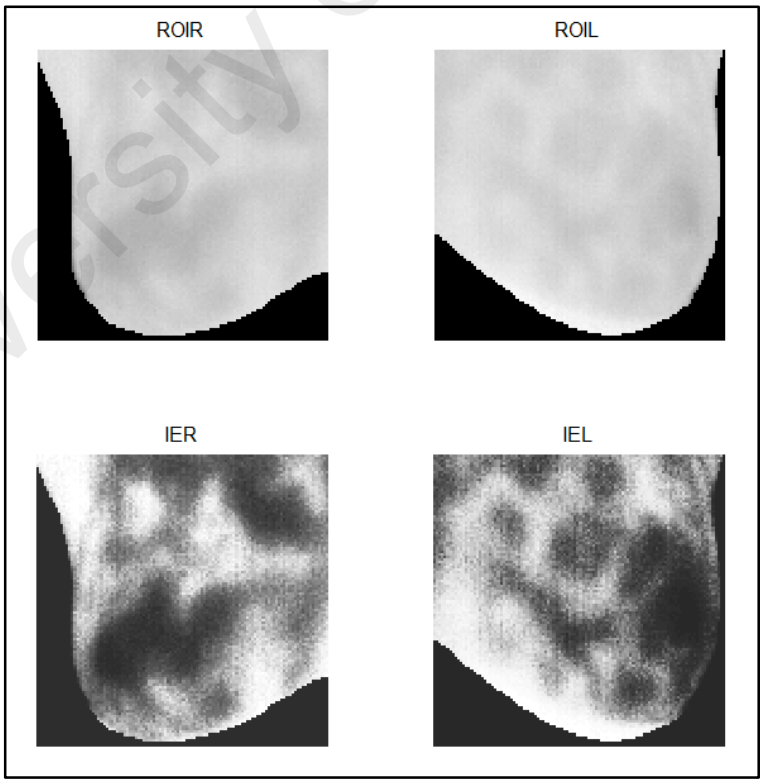

Figure 4.3: Original images and equalized images for Patient N30.

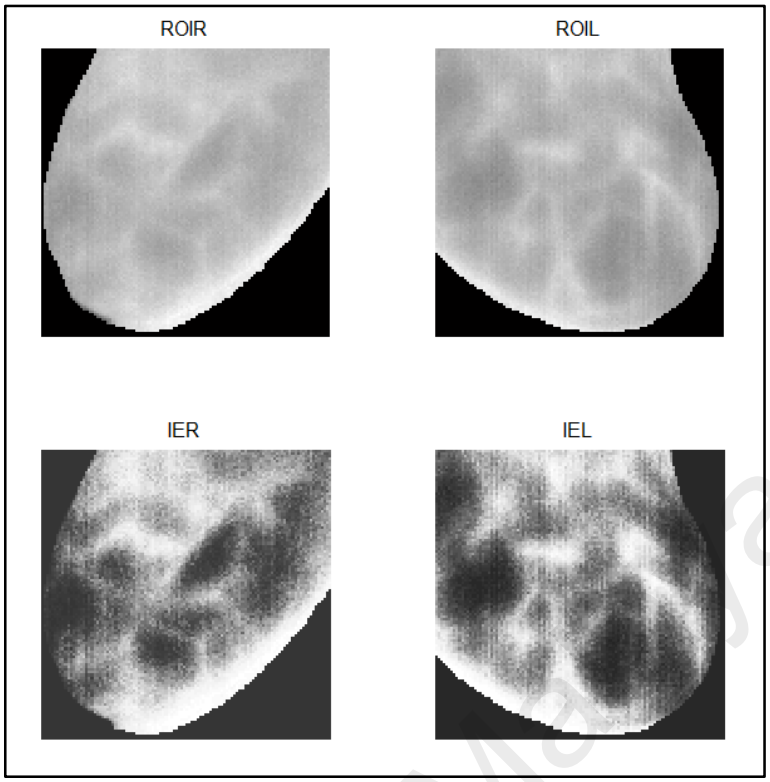

Figure 4.4: Original images and equalized images for Patient N38.

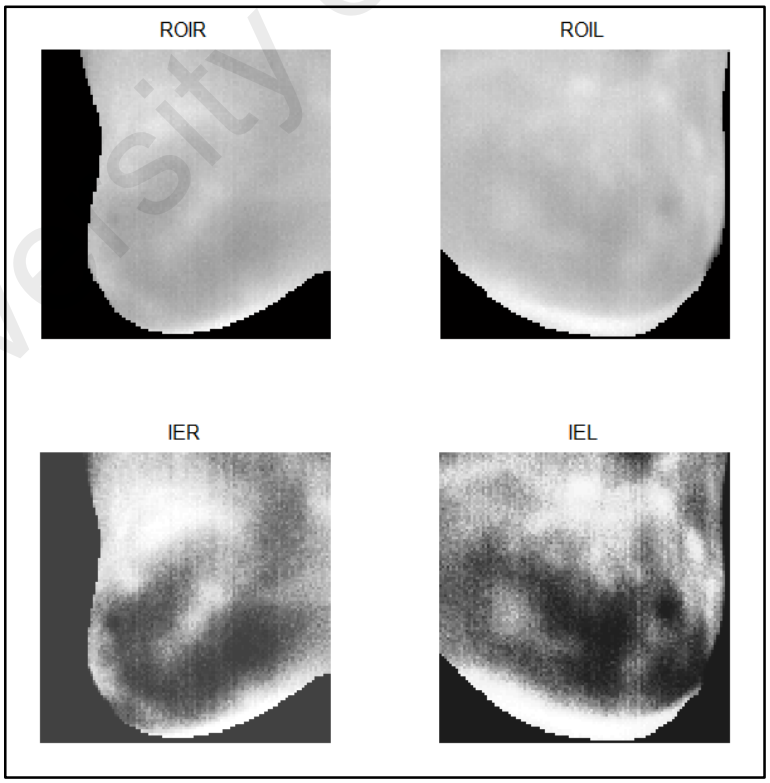

Figure 4.5: Original images and equalized images for Patient N45.

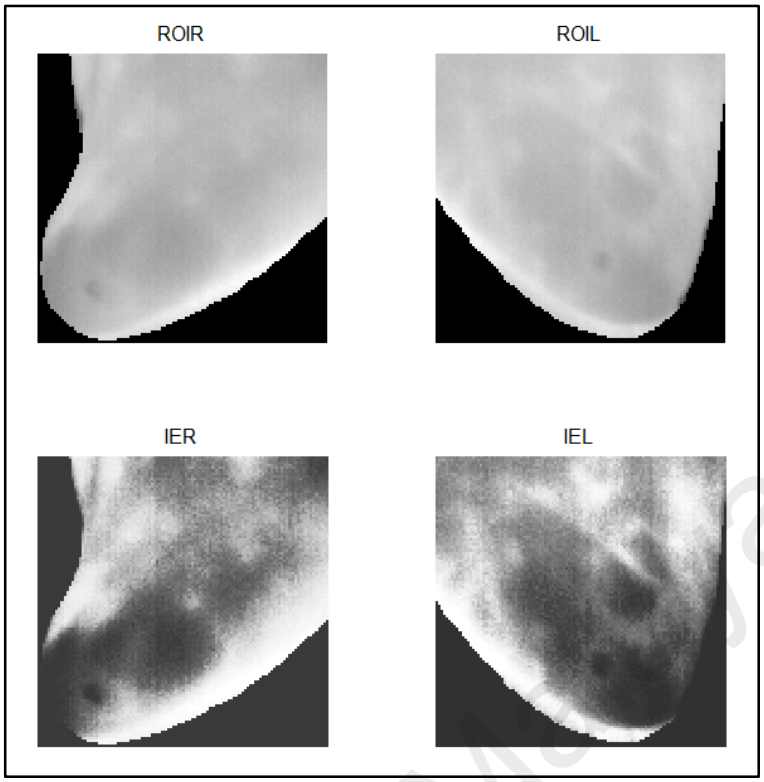

Figure 4.6: Original images and equalized images for Patient N53.

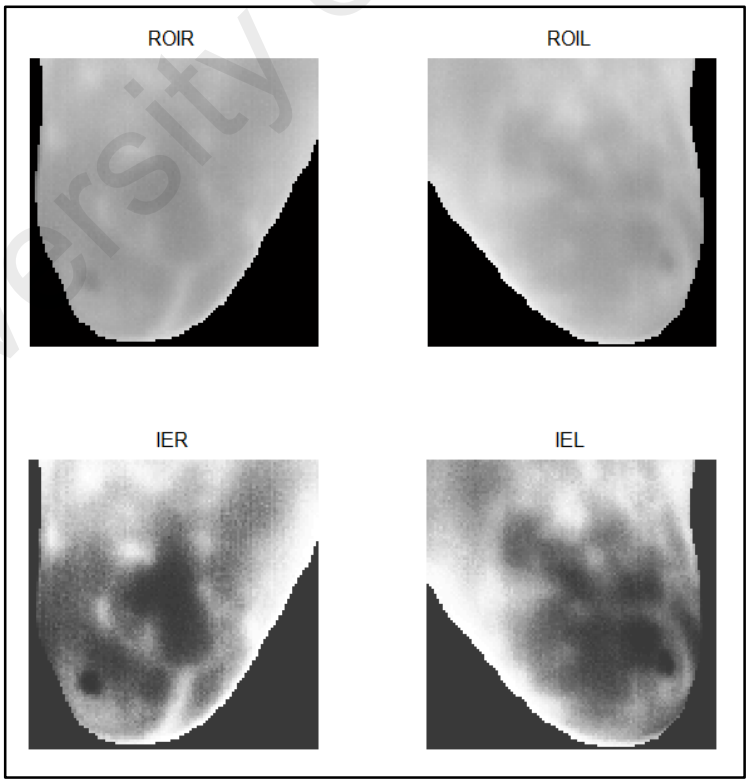

Figure 4.7: Original images and equalized images for Patient N60.

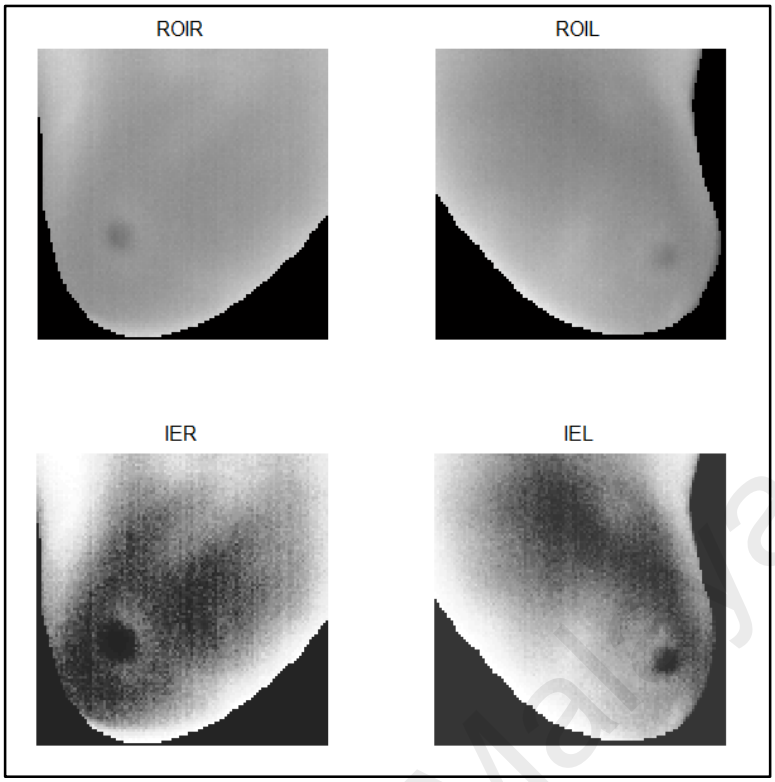

Figure 4.8: Original images and equalized images for Patient N68.

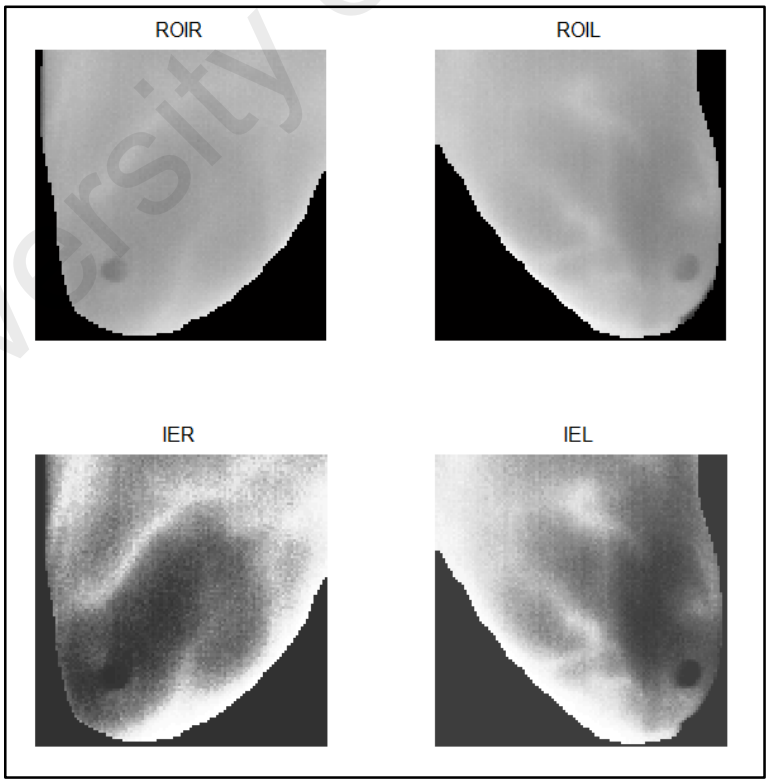

Figure 4.9: Original images and equalized images for Patient N75.

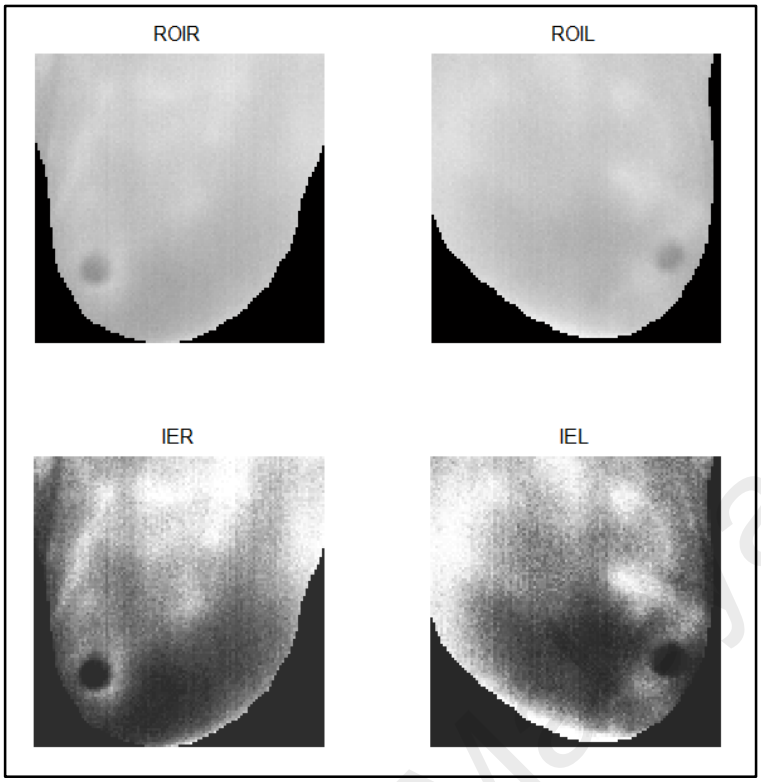

Figure 4.10: Original images and equalized images for Patient N90.

4.1.2 Result From Abnormal Cases

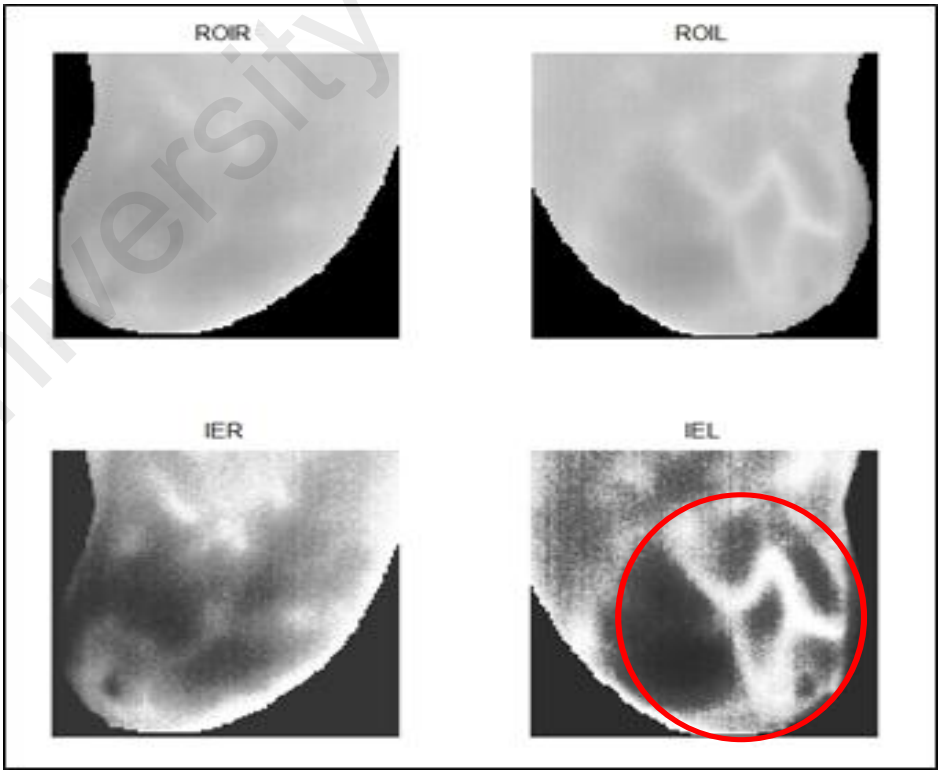

Figure 4.11: Original images and equalized images for Patient A08.

Patient A08 were diagnosed with cancer on her left breast. As shown by red circle in Figure 4.11, an area with high intensity value can be observed in IEL compare to IER.

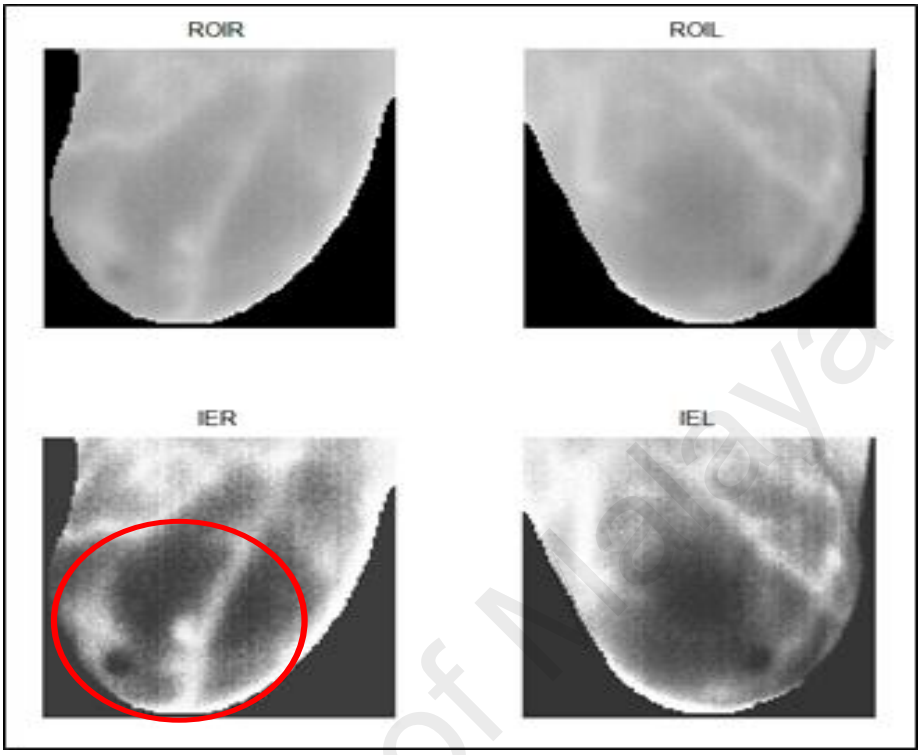

Figure 4.12: Original images and equalized images for Patient A10.

Patient A10 were diagnosed with cancer on her right breast. As shown by red circle in Figure 4.12, an area with high intensity value can be observed in IER compare to IEL.

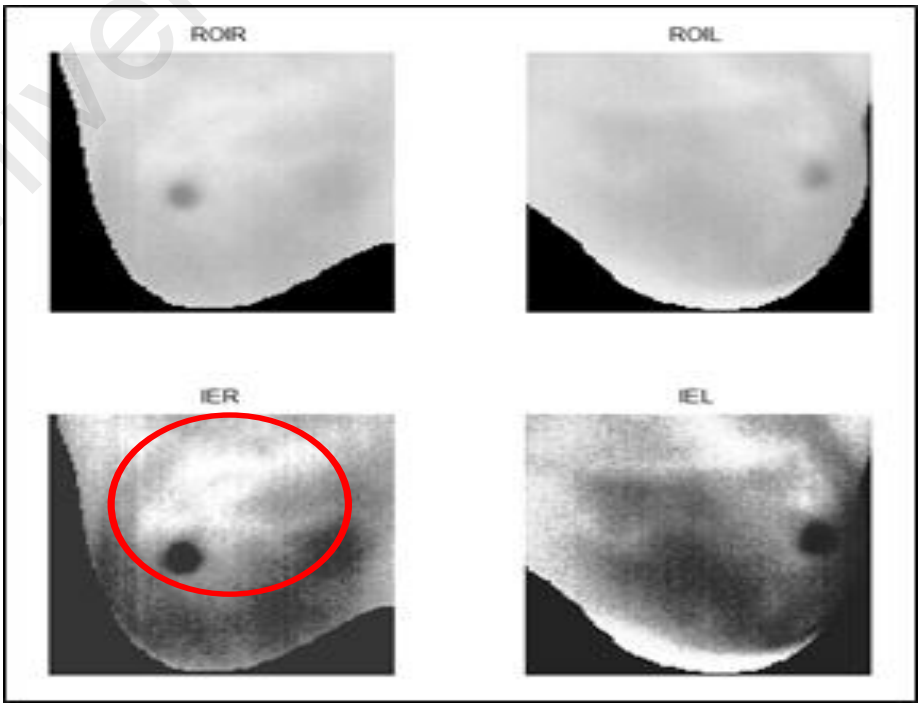

Figure 4.13: Original images and equalized images for Patient A22.

Patient A22 were diagnosed with cancer on her right breast. As shown by red circle in Figure 4.13, an area with high intensity value can be observed in IER compare to IEL.

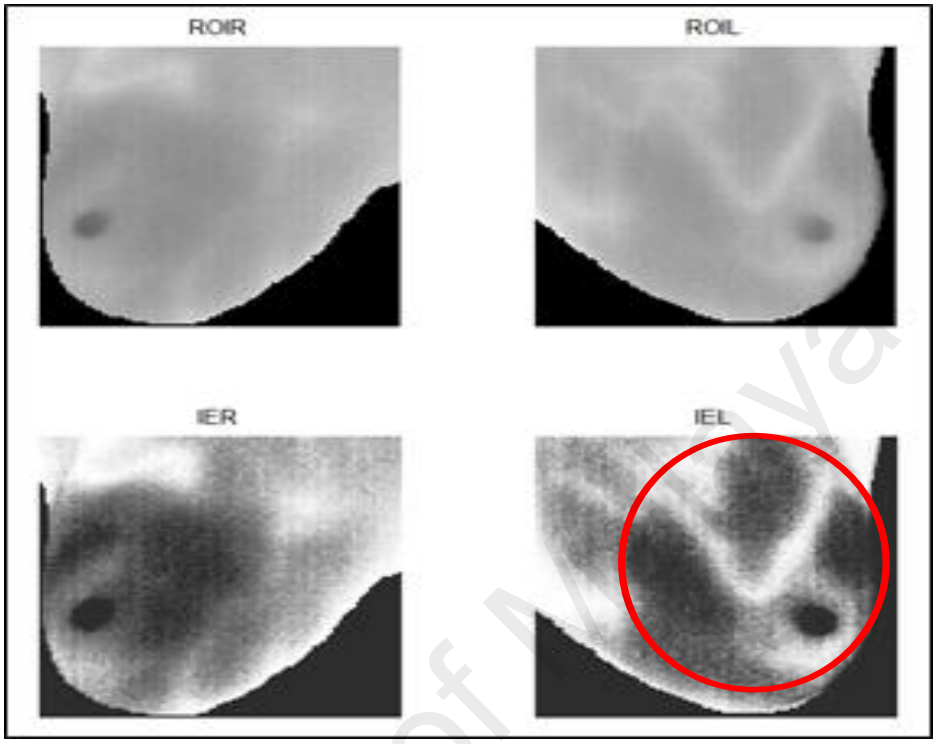

Figure 4.14: Original images and equalized images for Patient A24.

Patient A24 were diagnosed with cancer on her left breast. As shown by red circle in Figure 4.14, an area with high intensity value can be observed in IEL compare to IER.

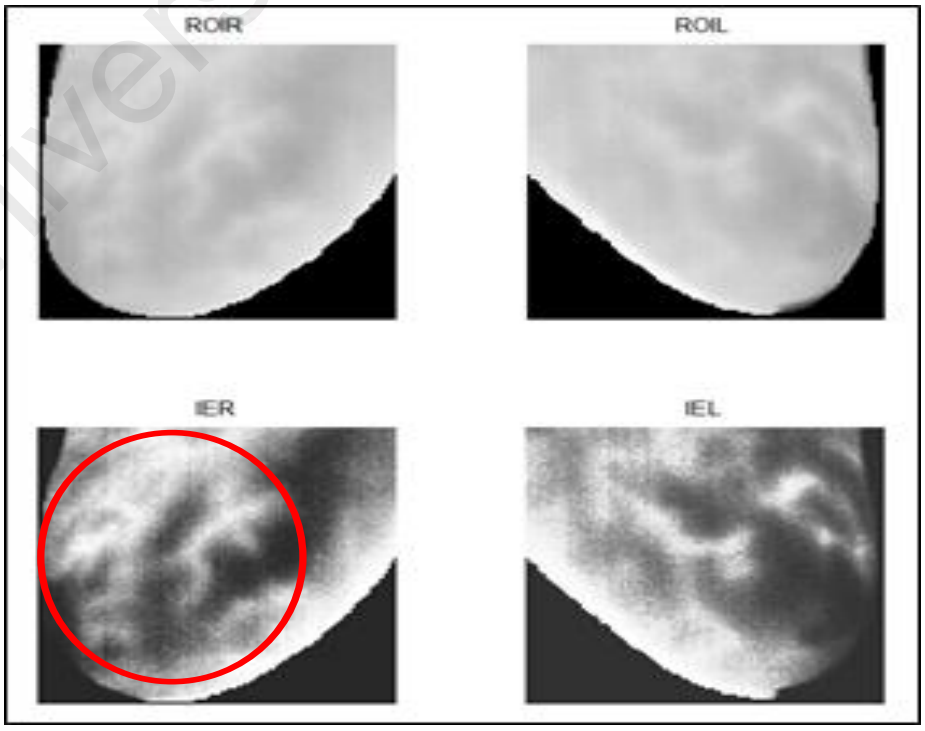

Figure 4.15: Original images and equalized images for Patient A30.

Patient A30 were diagnosed with cancer on her right breast. As shown by red circle in Figure 4.15, an area with high intensity value can be observed in IER compare to IEL.

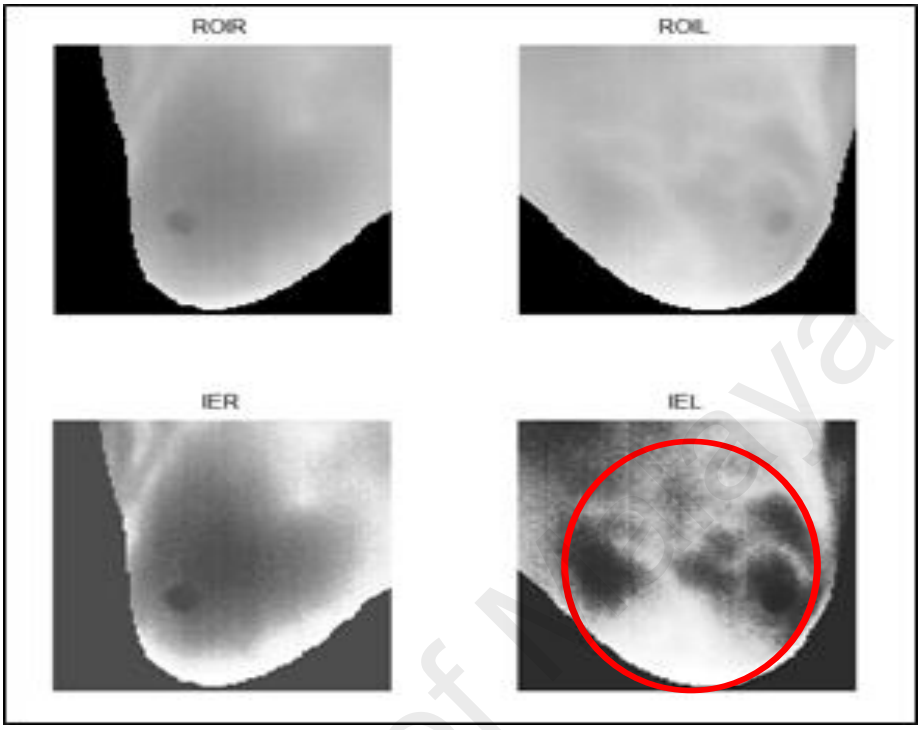

Figure 4.16: Original images and equalized images for Patient A32.

Patient A32 were diagnosed with cancer on her left breast. As shown by red circle in Figure 4.16, an area with high intensity value can be observed in IEL compare to IER.

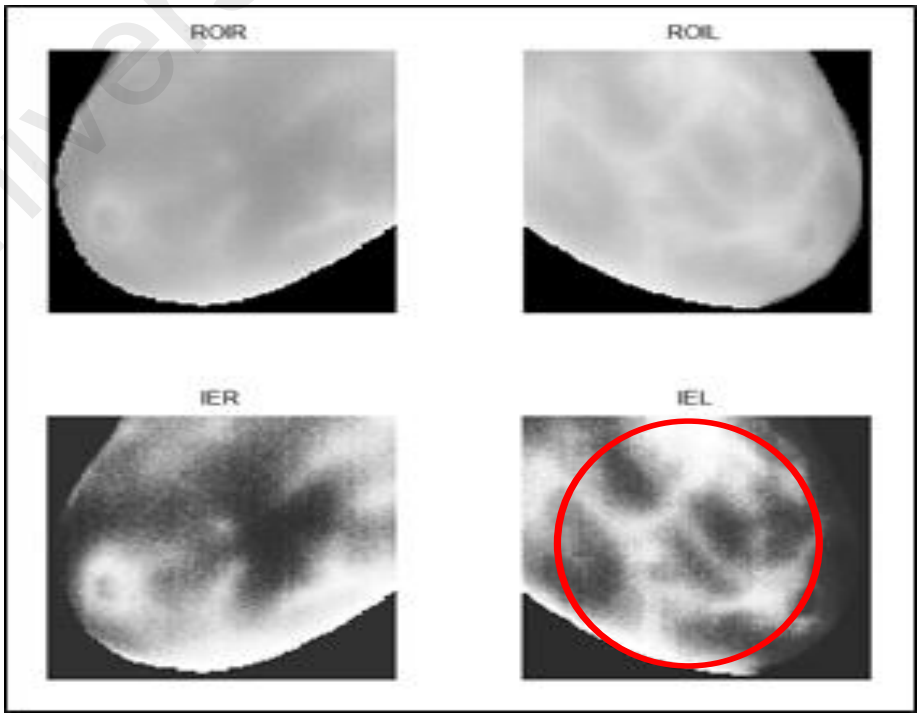

Figure 4.17: Original images and equalized images for Patient A34.

Patient A34 were diagnosed with cancer on her left breast. As shown by red circle in Figure 4.17, an area with high intensity value can be observed in IEL compare to IER.

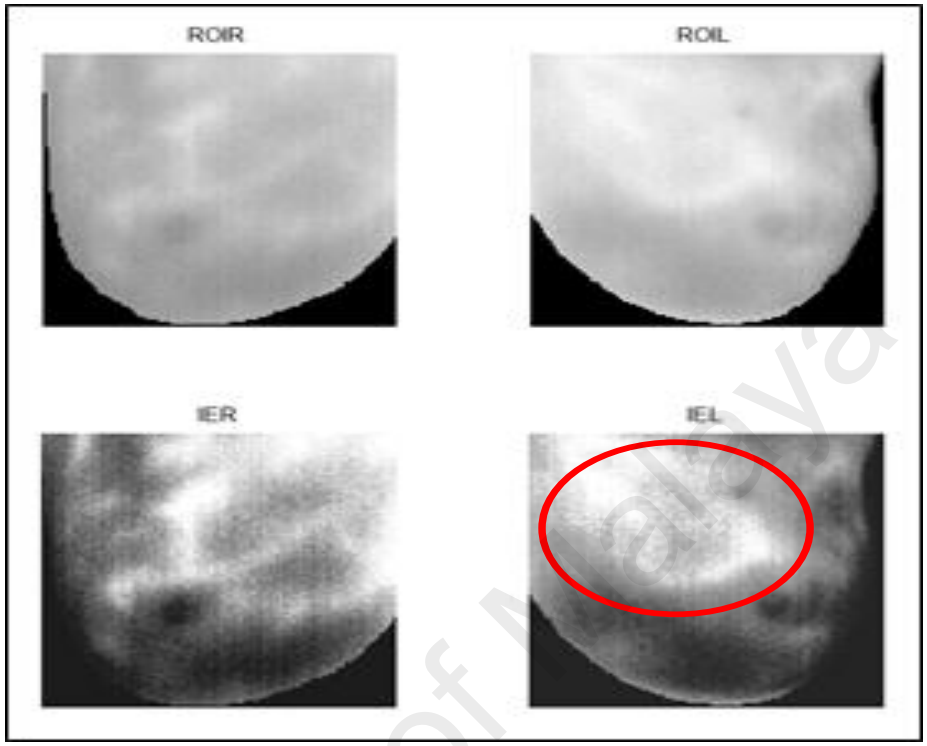

Figure 4.18: Original images and equalized images for Patient A42.

Patient A42 were diagnosed with cancer on her left breast. As shown by red circle in Figure 4.18, an area with high intensity value can be observed in IEL compare to IER.

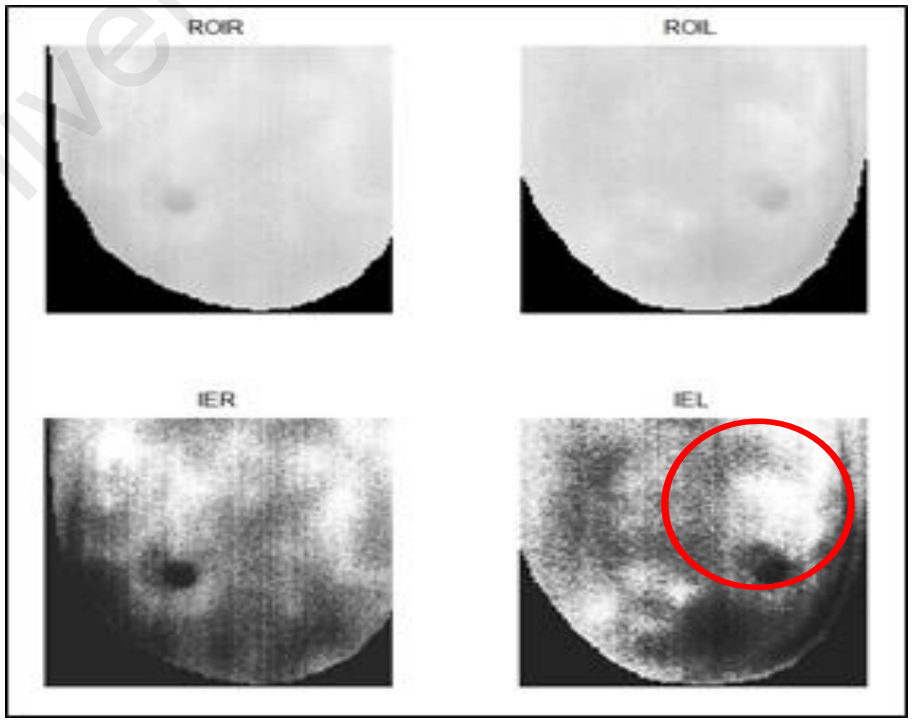

Figure 4.19: Original images and equalized images for Patient A44.

Patient A44 were diagnosed with cancer on her left breast. As shown by red circle in Figure 4.19, an area with high intensity value can be observed in IEL compare to IER.

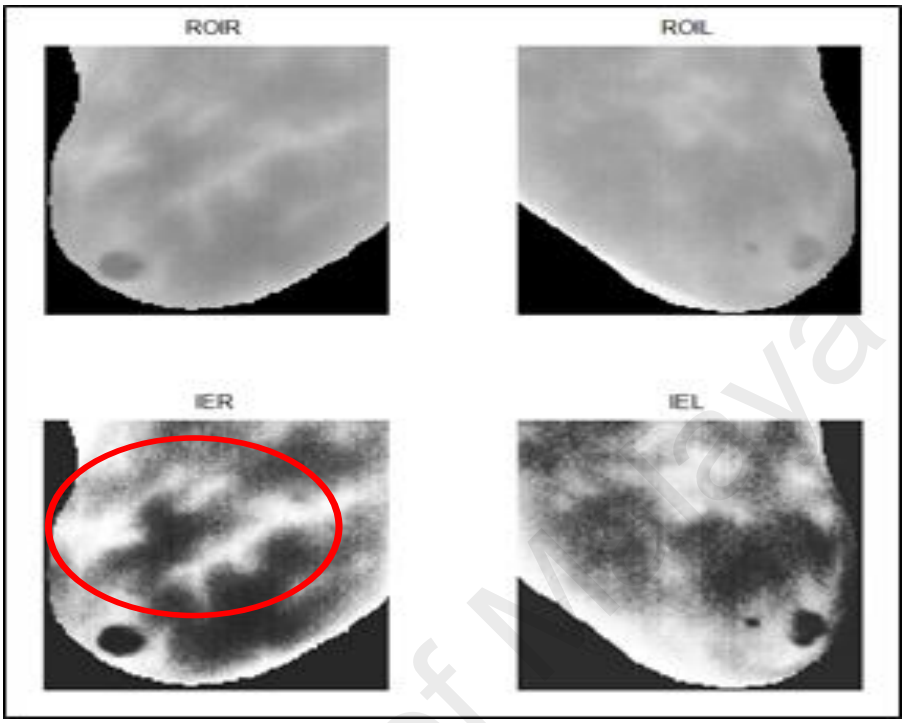

Figure 4.20: Original images and equalized images for Patient A46.

Patient A46 were diagnosed with cancer on her right breast. As shown by red circle in Figure 4.20, an area with high intensity value can be observed in IER compare to IEL.

4.1.3 Summary

The local contrast level of greyscale thermography image is low, as shown in ROIR and ROIL in Figure 4.1 until Figure 4.20. Therefore, the HE were used to spread the most frequent intensity value in ROIR and ROIL to increase the contrast of the image.

As shown in Figure 4.1 until Figure 4.10, the intensity pattern among all the normal patients are different regardless before and after HE. However, when compare intensity pattern between ROIR and ROIL for each patient, in most cases, the intensity value distribution is almost equal before and after HE. The reason was there is no unexpected high intensity captured in any ROI which indicate unexpected high surface temperature cause by cancer cells. However, in some cases, the distribution will be visually unequal, for example Patient N30 shown in Figure 4.3. These might cause by inflammation on the

patient skin surface which influence the heat release from the body or ointment application that give out heat. The change of body surface heat pattern will automatically alter the intensity pattern captured by thermal camera. For abnormal case, the high intensity indicating the possible area of cancer is highlighted clearly compare to before HE, as shown by oval shape red marker in Figure 4.11 until Figure 4.20. The location for each area were also varied from one patient to the other.

The unexpected high intensity in normal patient IER and IEL may cause wrong diagnose if features extracted directly from this image. Features extracted need to produce results that can generate differences between visually symmetrical and visually asymmetrical normal images with the abnormal images. Therefore, by using the new intensity level from image IEL and IER, the Chi-Squared distance, EMD and contrast measurement features were extracted by computing the distance and the contrast value between intensity levels using the equation shown in Chapter 3.

4.2 Features Analysis

From the feature extraction process, 6 sets of result data collected. Set one contains 40 Chi-squared distance value computed from abnormal patient images. Set two contains 40 EMD distance value computed from abnormal patient images. Set three contains 40 contrast measurement value computed from abnormal patient images. Set four contains 90 Chi-squared distance value computed from normal patient images. Set five contains 90 EMD distance value computed from normal patient images. Set six contains 90 contrast measurement value computed from normal patient images. Each set, then will be tested in pair. Hence, each set is divided into two similar number of data group, namely Group 1 and Group 2. This dataset divides based on the ROI contrast level in every image with Group 1 representing data from images with lower ROI contrast value and Group 2 representing data from images with higher ROI contrast value. The mean and standard deviation for each group from each dataset, later used as the input for the paired t-test.

Table 4.1 and Table 4.2 show the mean and standard deviation calculated for each group from each dataset.

The features tested using the paired t-test to analyse whether the values are statistically significance for classification. The null hypothesis for the t-test are: 1) the difference between two sides of breast for selected features' mean are statistically significant for abnormal patient and 2) the difference between two sides of breast for selected features' mean are statistically significant for normal patient. The significance value is set as 5%. The computed *p* value represents the probability for the observed difference to occur by chance. If the *p* value is less than the significance value, it means the null hypothesis is accepted where the observed difference unlikely happens by chance. Hence, the difference is statistically significant. Table 4.1 shows the result of paired t-test for abnormal patient and Table 4.2 shows the result paired t-test for normal patient. The range of critical values ranges from 0.2705 to 0.2853 for 90 normal samples with confidence level 0.05 and the range of critical values ranges from 0.2693 to 0.2859 for 50 abnormal samples with confidence level 0.05.

Table 4.1: Paired t-test result for abnormal patient.

Features		Abnormal (sample sizes = 50)		Paired t-test	**D'Agostinon Normality Test using D statistic** $\boldsymbol{D_{critical} = [0.2693, 0.2859]}$
		Mean	Standard Deviation		
Chi-squared Distance (defined in (8) with C=1)	Group 1	1.1680	0.1093	0.0022	D=0.2726
	Group 2	2.3230	0.3347		D=0.2695
EMD	Group 1	0.1432	0.0363	0.0061	D=0.2754
	Group 2	0.1975	0.0339		D=0.2732
Contrast Measurement	Group 1	0.1631	0.0312	0.0282	D=0.2788
	Group 2	0.2078	0.0185		D=0.2867

Table 4.2: Paired t-test result for normal patient.

Features		Normal (sample sizes = 90)		Paired t-test	**D'Agostinon Normality Test using D statistic** $D_{critical} = [0.2705, 0.2853]$
		Mean	Standard Deviation		
Chi-squared Distance (defined in (8) with C=1)	Group 1	1.1945	0.1071	0.1736	D=0.2821
	Group 2	1.3241	0.1076		D=0.2833
EMD	Group 1	0.1532	0.0219	0.0383	D=0.2712
	Group 2	0.1578	0.0234		D=0.2783
Contrast Measurement	Group 1	0.1698	0.0103	0.3721	D=0.2829
	Group 2	0.3875	0.4437		D=0.2831

4.2.1 Chi-Squared Distance

From the result for Chi-squared Distance features in Table 4.1, the p value of paired t-test is 0.0022 which is less than 0.05. It indicates that the observed difference between two sides of breast for this particular feature of contrast is unlikely to happen by chance. Therefore, the null hypothesis is accepted such that the observed difference is statistically significant. The normality test shows that the distributions for both groups are distributed normally. From the result of Chi-squared Distance in Table 4.2, the p value of paired t-test is 0.1736 which is more than 0.05. It indicates that the observed difference between two sides of breast for this particular feature of contrast is very likely to have happened by chance. Therefore, the null hypothesis is rejected such that the observed difference is statistically insignificant.

4.2.2 Earth Mover Distance

From the result of EMD in Table 4.1, the p value of paired t-test is 0.0061 which is less than 0.05. It indicates that the observed difference between two sides of breast for this particular feature of contrast is unlikely to happen by chance. Therefore, the null hypothesis is accepted such that the observed difference is statistically significant. The normality test shows that the distributions for both groups are distributed normally. From the result of contrast in Table 4.2, the p value of paired t-test is 0.0383 which is less than

0.05. It indicates that the observed difference between two sides of breast for this particular feature of contrast is very unlikely to have happened by chance.

4.2.3 Contrast Measurement

From the result of contrast measurement in Table 4.1, the p value of paired t-test is 0.0282 which is less than 0.05. It indicates that the observed difference between two sides of breast for this particular feature of contrast is unlikely to happen by chance. Therefore, the null hypothesis is accepted such that the observed difference is statistically significant. The normality test shows that the distributions for both groups are distributed normally. From the result of contrast measurement in Table 4.2, the p value of paired t-test is 0.3721 which is more than 0.05. It indicates that the observed difference between two sides of breast for this particular feature of contrast is very likely to have happened by chance. Therefore, the null hypothesis is rejected such that the observed difference is statistically insignificant.

4.2.4 Summary

Based on the results, the null hypothesis of Chi-squared distance are rejected for normal case and accepted for abnormal case. This indicates that Chi-squared distance is statistically significant to differentiate between normal and abnormal group. Meanwhile, for contrast measurement, the null hypothesis also rejected for normal cases and accepted for abnormal case. The difference hypothesis result shows the features significance to be used in classification image into normal and abnormal group. On the other hand, for both abnormal and normal cases, the EMD paired t-test p values are less than 0.05 which indicates the acceptance of null hypothesis for both cases. Therefore, EMD might not be a good indicator for detecting abnormalities despite the p value for abnormal case is much lower comparing to its normal case.

CHAPTER 5: CONCLUSION

5.1 Conclusion

The main indication of breast cancer detection using thermography is the difference between the left and right breast. However, in some cases, the difference is visually difficult to be detected due to the lack of contrast in the image. Therefore, a computer aided detection (CAD) system is designed to help differentiate between a breast with suspected breast cancer and a normal breast. The stages involve designing a CAD system is image pre-processing, image processing, features extraction and image classification. This study was done to extract suitable difference based features for future image classification into normal or abnormal group. Firstly, the left and right ROI were extracted manually to ensure the extraction only involve the breast area as most breast cancer cases occur within this area. The image then processed using Histogram Equalization to improve the contrast of the image followed by feature extraction. There are multiple features can be extracted from both ROI, however the focus are the three features which are Chi-Squared distance, EMD and contrast measurement. The feature values were later tested whether it is significant to differentiate the images into normal and abnormal classes using a statistical t-test.

As a conclusion, this study has meet the main objective to extract features for normal and abnormal breast thermography image classification with three texture features extracted from normal and abnormal patient images. The Chi-squared distance value, EMD distance value and contrast measurement value represent the difference between ROIL and ROIR for each image respectively based on the calculation stated in Chapter 3. Two out of three texture features tested in this study are statistically significant to categorize images into normal group and abnormal group. The two features are Chi-squared distance and contrast measurement features. The p-value result for Chi-squared distance for abnormal patients is 0.0022 which is less than 0.05 and for normal patients

is 0.1736 which is higher than 0.05. Therefore, the null hypothesis is rejected in normal cases and accepted for abnormal cases. For contrast measurement, the p-value for abnormal patients is 0.0282 which is less than 0.05 and for normal patients is 0.3721 which is more than 0.05. The null hypothesis also rejected in normal cases and accepted for abnormal cases. The different outcome for normal and abnormal group for both features indicates both features are significances for classification.

5.2 Recommendation / Future Work

Following are some suggestions for further work to be done:

1. An automatic segmentation can be implemented to replace the manual cropping suggested in this study. An automatic segmentation allows larger areas to be segmented including breast upper part as several breast cancer cases started near the muscle area above the breast.
2. Image classification should be made in the future to calculate the accuracy of Chi-squared distance and contrast measurement features in classifying the image into normal and abnormal image. Image classification is the last stage in CAD system design.
3. Another suggestion is to use the temperature matrix as an input to analyse thermography images besides the greyscale image. Temperature matrices are matrices that shows the temperature captured for each pixel of the image. The analysis of thermal image and temperature matrix may increase the reliability of thermography to be used as an alternative clinical tool for breast cancer detection.

REFERENCES

Abdel-Nasser, M., Rashwan, H. A., Puig, D., & Moreno, A. (2015). Analysis of tissue abnormality and breast density in mammographic images using a uniform local directional pattern. *Expert Systems with Applications, 42*(24), 9499-9511. doi:10.1016/j.eswa.2015.07.072

Acharya, U. R., Ng, E. Y., Tan, J. H., & Sree, S. V. (2012). Thermography based breast cancer detection using texture features and Support Vector Machine. *J Med Syst, 36*(3), 1503-1510. doi:10.1007/s10916-010-9611-z

Araujo, M. C., Lima, R. C. F., & de Souza, R. (2014). Interval symbolic feature extraction for thermography breast cancer detection. *Expert Systems with Applications, 41*(15), 6728-6737. doi:10.1016/j.eswa.2014.04.027

Borchartt, T. B., Conci, A., Lima, R. C. F., Resmini, R., & Sanchez, A. (2013). Breast thermography from an image processing viewpoint: A survey. *Signal Processing, 93*(10), 2785-2803. doi:doi:10.1016/j.sigpro.2012.08.012

DeSantis, C. E., Bray, F., Ferlay, J., Lortet-Tieulent, J., Anderson, B. O., & Jemal, A. (2015). International Variation in Female Breast Cancer Incidence and Mortality Rates. *Cancer Epidemiology Biomarkers & Prevention, 24*(10), 1495-1506. doi:10.1158/1055-9965.epi-15-0535

EtehadTavakol, M., Chandran, V., Ng, E. Y. K., & Kafieh, R. (2013). Breast cancer detection from thermal images using bispectral invariant features. *International Journal of Thermal Sciences, 69*, 21-36. doi: 10.1016/j.ijthermalsci.2013.03.001

Etehadtavakol, M., Ng, E. Y. K., Chandran, V., & Rabbani, H. (2013). Separable and non-separable discrete wavelet transform based texture features and image classification of breast thermograms. *Infrared Physics & Technology, 61*, 274-286. doi:10.1016/j.infrared.2013.08.009

Ferlay, J., Soerjomataram, I., Dikshit, R., Eser, S., Mathers, C., Rebelo, M., . . . Bray, F. (2015). Cancer incidence and mortality worldwide: Sources, methods and major patterns in GLOBOCAN 2012. *International Journal of Cancer, 136*(5), E359-E386. doi:10.1002/ijc.29210

Francis, S. V., Sasikala, M., Bharathi, G. B., & Jaipurkar, S. D. (2014). Breast cancer detection in rotational thermography images using texture features. *Infrared Physics & Technology, 67*, 490-496.

Johnson, M. C., & Cutler, M. L. (2016). Anatomy and Physiology of the Breast. In I. Jatoi & A. Rody (Eds.), *Management of Breast Diseases* (pp. 1-39). Cham: Springer International Publishing.

Krawczyk, B., & Schaefer, G. (2014). Breast Thermogram Analysis Using Classifier Ensembles and Image Symmetry Features. *IEEE Systems Journal, 8*(3), 921-928. doi:10.1109/JSYST.2013.2283135

Lanisa, N., Cheok, N. S., & Wee, L. K. (2014). *Color morphology and segmentation of the breast thermography image.* Paper presented at the Biomedical Engineering and Sciences (IECBES), 2014 IEEE Conference on.

Marques, R. S., Resmini, R., Conci, A., Fontes, C. A. P., & Lima, R. C. F. (2012). Método para segmentação manual de imagens térmicas para geração de GroundTruth.

Medicine, J. H. (2014). Breast Cancer & Breast Pathology. Retrieved from http://pathology.jhu.edu/breast/anatomy.php

Moghbel, M., & Mashohor, S. (2013). A review of computer assisted detection/diagnosis (CAD) in breast thermography for breast cancer detection. *Artificial Intelligence Review, 39*(4), 305-313. doi:10.1007/s10462-011-9274-2

Mookiah, M. R. K., Acharya, U. R., & Ng, E. Y. K. (2012). Data mining technique for breast cancer detection in thermograms using hybrid feature extraction strategy.

Quantitative InfraRed Thermography Journal, 9(2), 151-165. doi:10.1080/17686733.2012.738788

Ng, E. Y. K. (2009). A review of thermography as promising non-invasive detection modality for breast tumor. *International Journal of Thermal Sciences, 48*(5), 849-859. doi:10.1016/j.ijthermalsci.2008.06.015

NG, E. Y. K., & KEE, E. C. (2007). INTEGRATIVE COMPUTER-AIDED DIAGNOSTIC WITH BREAST THERMOGRAM. *Journal of Mechanics in Medicine and Biology, 07*(01), 1-10. doi:10.1142/s0219519407002091

Onega, T., Beaber, E. F., Sprague, B. L., Barlow, W. E., Haas, J. S., Tosteson, A. N., . . . Geller, B. (2014). Breast cancer screening in an era of personalized regimens: A conceptual model and National Cancer Institute initiative for risk-based and preference-based approaches at a population level. *Cancer, 120*(19), 2955-2964.

Qi, H., & Diakides, N. (2009). Thermal Infrared Imaging in Early Breast Cancer Detection. In R. Hammoud (Ed.), *Augmented Vision Perception in Infrared* (pp. 139-152): Springer London.

Rachev, S. T. (1985). The Monge–Kantorovich Mass Transference Problem and Its Stochastic Applications. *Theory of Probability & Its Applications, 29*(4), 647-676. doi:10.1137/1129093

Rane, K. P., Joshi, R. R., & Chaudhari, L. A. (2014). *IR Imaging: A New Approach for Breast Cancer Detection*.

Schaefer, G. (2014). ACO classification of thermogram symmetry features for breast cancer diagnosis. *Memetic Computing, 6*(3), 207-212. doi:10.1007/s12293-014-0135-9

Schaefer, G., Závišek, M., & Nakashima, T. (2009). Thermography based breast cancer analysis using statistical features and fuzzy classification. *Pattern Recognition, 42*(6), 1133-1137. doi:10.1016/j.patcog.2008.08.007

Shanthi, S., & Murali Bhaskaran, V. (2014). A novel approach for classification of abnormalities in digitized mammograms. *Sadhana, 39*(5), 1141-1150. doi:10.1007/s12046-014-0278-x

Suganthi, S. S., & Ramakrishnan, S. (2014). Analysis of Breast Thermograms Using Gabor Wavelet Anisotropy Index. *Journal of Medical Systems, 38*(9), 1-7. doi:10.1007/s10916-014-0101-6

Wishart, G. C., Campisi, M., Boswell, M., Chapman, D., Shackleton, V., Iddles, S., . . . Britton, P. D. (2010a). The accuracy of digital infrared imaging for breast cancer detection in women undergoing breast biopsy. *European Journal of Surgical Oncology (EJSO), 36*(6), 535-540. doi: 10.1016/j.ejso.2010.04.003

Wishart, G. C., Campisi, M., Boswell, M., Chapman, D., Shackleton, V., Iddles, S., . . . Britton, P. D. (2010b). The accuracy of digital infrared imaging for breast cancer detection in women undergoing breast biopsy. *Ejso, 36*(6), 535-540. doi:10.1016/j.ejso.2010.04.003

Youlden, D. R., Cramb, S. M., Yip, C. H., & Baade, P. D. (2014). Incidence and mortality of female breast cancer in the Asia-Pacific region. *Cancer biology & medicine, 11*(2), 101-115.